Landauer-Büttiker approach for hyperfine mediated electronic transport in the integer quantum Hall regime

Aniket Singha,[1] M. H. Fauzi,[2] Y. Hirayama,[2] and Bhaskaran Muralidharan[1,*]

[1]*Department of Electrical Engineering, Indian Institute of Technology Bombay, Powai, Mumbai-400076, India*
[2]*Department of Physics, Graduate School of Science, Tohoku University, 6-3 Aramaki aza Aoba, Aoba-ku, Sendai, Miyagi-980-8578, Japan*

The interplay of spin-polarized electronic edge states with the dynamics of the host nuclei in quantum Hall systems presents rich and nontrivial transport physics. Here, we develop a Landauer-Büttiker approach to understand various experimental features observed in the integer quantum Hall setups featuring quantum point contacts. The approach developed here entails a phenomenological description of spin-resolved interedge scattering induced via hyperfine assisted electron-nuclear spin flip-flop processes. A self-consistent simulation framework between the nuclear spin dynamics and edge state electronic transport is presented in order to gain crucial insights into the dynamic nuclear polarization effects on electronic transport and in turn the electron-spin polarization effects on the nuclear spin dynamics. In particular, we show that the hysteresis noted experimentally in the conductance-voltage trace as well as in the resistively detected NMR line-shape results from a lack of quasiequilibrium between electronic transport and nuclear polarization evolution. In addition, we present circuit models to emulate such hyperfine mediated transport effects to further facilitate a clear understanding of the electronic transport processes occurring around the quantum point contact. Finally, we extend our model to account for the effects of quadrupolar splitting of nuclear levels and also depict the electronic transport signatures that arise from single and multiphoton processes.

I. INTRODUCTION

Nuclear spintronics concerns the manipulation of nuclear spins by means of hyperfine interaction between the host nuclei and the itinerant electrons and their read out using electronic transport [1] or optical [2] measurements. Quantum Hall geometries in both the integer [1,3–11] and the fractional regime [12–16] featuring gated quantum point contacts (QPC) offer a viable method for controlling the spin polarization of the electronic edge channels. This in turn facilitates the manipulation of the nuclear spins via a hyperfine mediated interplay between the spin-polarized edge states and the dynamics of the host nuclei. Such an interplay has revealed rich and nontrivial transport physics in the form of hysteresis in the observed conductance-voltage traces and nontrivial line shapes in the resistively detected NMR (RDNMR) traces [3–5,10,17]. Despite several advancements in the transport experiments involving such setups, theoretical models for hyperfine interaction mediated edge transport through the QPC in the Hall geometry are clearly missing in the current literature. The object of this work is hence to develop transport models that couple the dynamics of the host nuclei with edge channel electronic transport as an attempt to fill this gap and theoretically interpret various experiments with specific focus on the conductance-voltage traces [3] and the RDNMR line shapes [11,18–25].

We develop our transport models based on a modified Landauer-Büttiker formalism that includes a *spin-flip transmission coefficient*, which is nuclear polarization dependent and describes the rate of electron-nuclear spin flip-flops per unit energy around the QPC region. Using this approach, we show that the hysteresis noted in both the conductance and the RDNMR traces [3,11,18–25] results from a lack of steady state between electronic transport and nuclear polarization evolution and can be explained by taking into account the finite rate of electron-nuclear spin flip-flops in a source limited channel in addition to a finite nuclear spin-lattice relaxation time. The self-consistent simulation framework between the nuclear spin dynamics and the edge state electronic transport developed here offers crucial insights into the dynamic nuclear polarization effects on electronic transport and in turn the electron-spin polarization effects on the nuclear spin dynamics. In addition, we present circuit models to emulate such hyperfine mediated transport effects for a clear understanding of the phenomena occurring near the QPC. Finally, we also address the effects of quadrupolar splitting of the nuclear levels and depict the electronic transport signatures that arise from single and multiphoton absorption processes [17].

This paper is organized as follows. In Sec. II, we briefly detail the experimental setup and features that form our current focus after which we spell out the generic formalism. Specifically, in Sec. II B, a phenomenological model for hyperfine mediated transport through the QPC is developed in detail. Section III elucidates the results from the simulation framework developed with the specific focus on explaining the various experimental trends noted. Specifically, Sec. III A is devoted to the understanding of the hysteritic conductance voltage traces noted for different filling factors and Sec. III B deals with the RDNMR line-shape features in great detail.

II. EXPERIMENTAL DETAILS AND THEORETICAL DESCRIPTION

In the schematic of the experimental setup shown in Fig. 1(a), an appropriately gated single QPC is utilized to selectively filter out a single spin channel into the region
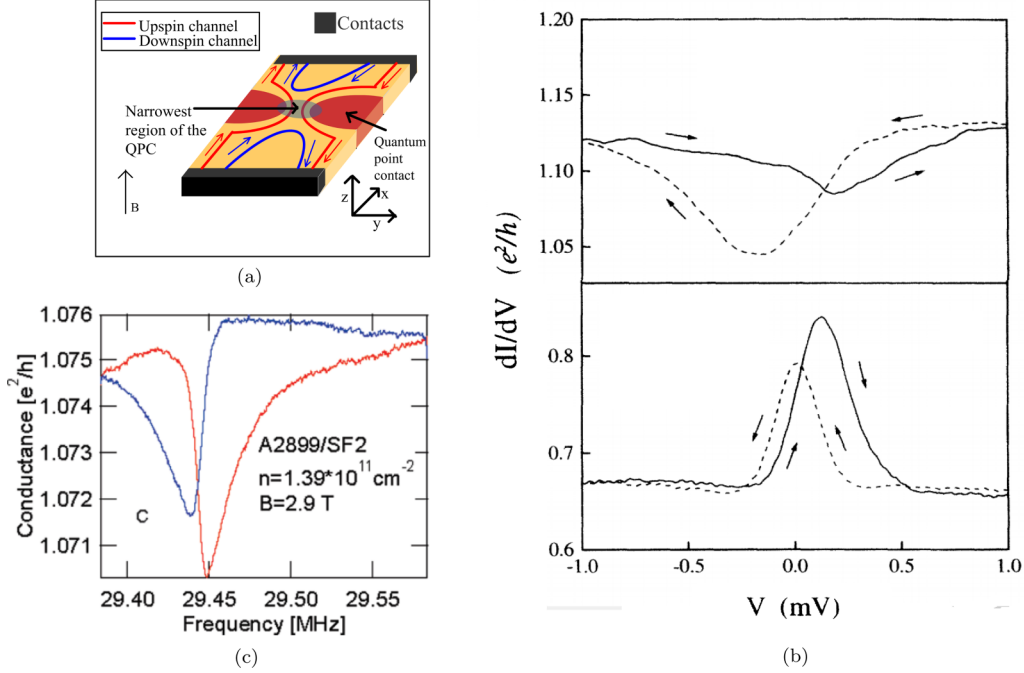
*bm@ee.iitb.ac.in

FIG. 1. Experimental details. (a) Schematic of the spin channels propagating through the quantum Hall device with a single QPC for the case $G = e^2/h$. (b) Experimental traces (reproduced with permission from Ref. [3]) of the differential conductance dI/dV vs voltage V for $dI/dV > e^2/h$ (top), $dI/dV < e^2/h$ (bottom) measured on a single QPC at $T = 50$ mK and $B = 5.4$ T. Solid curve: forward sweep, dashed curve: backward sweep. Round-trip sweep time for each trace is 200 s. (c) Experimental traces (reproduced with permission from Ref. [11]) of the Hall conductance change and hysteresis in the Hall conductance in a GaAs sample with RF frequency sweep measured at $B = 2.9$ T and $T = 30$ mK.

beyond the QPC thereby creating an imbalance between the up-spin channel and the down-spin channel. The principal experimental signature here is the change in conductance with voltage sweep near $V = 0$ [3] as shown in Fig. 1(b) as well as the change in Hall resistance with RF frequency sweep (also known as resistively detected NMR or RDNMR) [11] as shown in Fig. 1(c). Along with the change in the conductance, another feature that has attracted significant attention is the hysteresis in the conductance plots during forward and reverse voltage or RF frequency sweep as shown in Figs. 1(b) and 1(c), respectively. A compact theoretical model to elaborate the physics of such a conductance modulation as well as hysteresis occurring in the gated QPC set up forms the primary focus of this work.

An accurate modeling of such phenomena involves taking into account the details of wave-function correlations via the density matrix approach [26]. Mathematical modeling of such hyperfine mediated electron transport process self-consistently with evolution of the nuclear polarization from the density matrix formalism [26] is complicated and computationally heavy. In this paper, we thus adapt a computationally efficient phenomenological model to account for such hyperfine mediated electronic transport through the QPC.

We now provide a theoretical description of the nuclear spin dynamics coupled to the electronic transport following which we focus on how to apply this to our specific set up. We begin with the description of the nuclear spin dynamics by formulating a master equation in the nuclear spin space followed by the description of the extended Landauer-Büttiker formalism for the edge state electronic transport.

A. Description of scattering processes

In order to describe the electron-nuclear hyperfine interaction, we start with the Fermi contact hyperfine interaction Hamiltonian for the case with nonvarying electronic density of states in space, given by [2]

$$\hat{H}_{\text{HF}}(\mathbf{r}_n) = \sum_n A_{\text{eff}} \psi^*(\mathbf{r}_n)\psi(\mathbf{r_n})a_0^3$$
$$\times \left[\hat{\mathbf{S}}_{\mathbf{z}} \otimes \hat{\mathbf{I}}_{\mathbf{z}}^{\mathbf{n}} + \left\{ \frac{\hat{\mathbf{I}}_+^{\mathbf{n}} \otimes \hat{\mathbf{S}}_- + \hat{\mathbf{S}}_+ \otimes \hat{\mathbf{I}}_-^{\mathbf{n}}}{2} \right\} \right], \quad (1)$$

where $\psi(\mathbf{r_n})$ represents the electron wave function at the point $\mathbf{r_n}$, with $\psi^*(\mathbf{r_n})\psi(\mathbf{r_n})$ representing the effective electron density per unit volume at the point $\mathbf{r_n}$, A_{eff} is the effective hyperfine coupling constant, $\hat{S}_z, \hat{I}_z^n$ are the operators representing the z component of the electronic spin and the nuclear spin respectively, with a_0^3 representing a unit cell volume. The operator "$\otimes$" represents the tensor product between the electron spin and the nuclear spin spaces. The operators $\hat{S}_{+(-)}$ and $\hat{I}_{+(-)}^n$ are the corresponding spin raising (lowering) operators for the electron and the nuclear spins, respectively. The above equation assumes $\psi_\uparrow(\mathbf{r_n}) = \psi_\downarrow(\mathbf{r_n}) = \psi(\mathbf{r_n})$, where "$\uparrow$" and "$\downarrow$" represents the eigenstates in the electron spin-space. In the quantum Hall regime, however, the eigenstates are localized in space along the transverse direction. In this case, $\psi_\uparrow(\mathbf{r_n}) \neq \psi_\downarrow(\mathbf{r_n})$ and thus the Hamiltonian should be

recast in the form [27–29]

$$\hat{H}_{\text{HF}}(\mathbf{r}_n)$$

$$= A_{\text{eff}} a_0^3 \sum_{|\phi,\beta\rangle\langle\varphi,\alpha|} \langle\phi,\beta| \left[\hat{\mathbf{S}}_{\mathbf{z}} \otimes \hat{\mathbf{I}}_{\mathbf{z}}^{\mathbf{n}} + \left\{ \frac{\hat{\mathbf{I}}_+^{\mathbf{n}} \otimes \hat{\mathbf{S}}_- + \hat{\mathbf{S}}_+ \otimes \hat{\mathbf{I}}_-^{\mathbf{n}}}{2} \right\} \right]$$

$$\times |\varphi,\alpha\rangle \times \sum_n \{\langle\psi_\beta|\mathbf{r}_n\rangle|\phi,\beta\rangle\langle\varphi,\alpha|\langle\mathbf{r}_n|\psi_\alpha\rangle\}, \quad (2)$$

where $|\phi,\beta\rangle = |\phi\rangle \otimes |\beta\rangle$ and $|\varphi,\alpha\rangle = |\varphi\rangle \otimes |\alpha\rangle$ with $|\alpha\rangle$ and $|\beta\rangle$ belonging to the electron spin-space and $|\phi\rangle$ and $|\varphi\rangle$ belonging to the nuclear-spin space in the presence of a magnetic field pointing along the z direction.

When the coupling constant A_{eff} is small, the effect of the two terms in (1) can be separated. The first term results in an effective magnetic field and the second term within the curly brackets represents the electron-nuclear spin flip-flop processes. The first term in (1), which also corresponds to $|\alpha\rangle = |\beta\rangle$ and $|\phi\rangle = |\varphi\rangle$ in (2) introduces an additional shift in the electronic energy levels as well as between states of different nuclear spins. The electronic energy difference Δ between the up-spin channel electrons and the down-spin channel electrons is given by [30]

$$\Delta = g_{\text{el}}\mu_B B_{\text{app}} + A_{\text{eff}}\langle I_z\rangle, \quad (3)$$

where g_{el}, μ_B, and B_{app} are the effective Lande g-factor of the electron in GaAs, the Bohr magneton, and the applied magnetic field respectively. The above expression is obtained by assuming an isotropic nuclear spin distribution. Similarly, the energy difference ϵ between the adjacent nuclear spin states differing by a magnetic quantum number of $\Delta s = \pm 1$ is given by

$$\epsilon = g_{\text{nuc}}\mu_B^{\text{nuc}} B_{\text{app}} + A''\langle S_z\rangle, \quad (4)$$

where g_{nuc} is the effective Lande g factor of the nuclide in consideration and μ_B^{nuc} is the nuclear Bohr magneton. The effective coupling constant $A'' = A_{\text{eff}} a_0^3 n_{\text{el}}$ [2,30,31], where n_{el} is the electronic carrier density. The magnetic quantum number for the GaAs nuclei varies from $-3/2$ to $+3/2$ in steps of $\Delta s = +1$. In standard literature, the second terms in (3) and (4) represent the Overhauser shift and the Knight shift, respectively. However, for practical purposes, $g_{\text{nuc}} \ll g_{\text{el}}$ and $A'' \ll A_{\text{eff}}$ and hence ϵ may be neglected with respect to Δ and the nuclear spin flips may be considered elastic.

The electron-nuclear spin flip-flop processes are described by the second term in the Hamiltonian in (1), which also corresponds to $|\alpha\rangle \neq |\beta\rangle$ and $|\phi\rangle \neq |\varphi\rangle$ in (2) and the scattering rates are evaluated via the Fermi's golden rule [32,33], typically related to the densities of the initial and the final states. In this case, the electronic wave-function distribution $\psi_\alpha(\mathbf{r}_n)$ and $\psi_\beta(\mathbf{r}_n)$ overlaps with the nuclear wave function on each site $\mathbf{r}_n$ differently, and this effect is accounted for via the overlap terms $\psi_\beta^*(\mathbf{r_n})\psi_\alpha(\mathbf{r_n})$ for up to down or down to up electronic spin transitions. The procedure for a self-consistent description of electronic transport coupled to hyperfine spin dynamics then entails the time-dependent simulation of the nuclear spin dynamics, with the electronic transport processes in steady state. This is because the nuclear spin dynamics are typically slow due to slow relaxation rates, slow diffusion rates as well as longer flip-flop times in comparison with the

electronic transport velocities. The nuclear spin dynamics at each point $\mathbf{r}_n$ are dictated via the electron-nuclear hyperfine flip rates calculated from the Fermi's golden rule [32] given by

$$\Gamma_{\uparrow\downarrow}(\mathbf{r}_n) = \frac{2\pi}{\hbar}|A_{\text{eff}}|^2 \int dE\, n_\uparrow(\mathbf{r}_n, E) p_\downarrow(\mathbf{r}_n, E)$$

$$\Gamma_{\downarrow\uparrow}(\mathbf{r}_n) = \frac{2\pi}{\hbar}|A_{\text{eff}}|^2 \int dE\, n_\downarrow(\mathbf{r}_n, E) p_\uparrow(\mathbf{r}_n, E), \quad (5)$$

where $\Gamma_{\downarrow\uparrow}(\mathbf{r}_n)$ [$\Gamma_{\uparrow\downarrow}(\mathbf{r}_n)$] represents the up to down (down to up) nuclear spin transition rate at the nuclear co-ordinate $\mathbf{r}_n$ between magnetic quantum numbers that differ by $+1$ (-1) in the nuclear spin space due to flip-flop transitions of electrons at energy E. The quantities $n_\uparrow(\mathbf{r}_n, E)$ and $n_\downarrow(\mathbf{r}_n, E)$ [$p_\uparrow(\mathbf{r}_n, E)$ and $p_\downarrow(\mathbf{r}_n, E)$] denote the densities of filled (vacant) states per unit energy per unit area at the point $\mathbf{r}_n$. The up to down (down to up) electronic spin transition rate based on (5) depends not only on the availability of electrons in the up (down) spin density of states $D_{\uparrow(\downarrow)}(\mathbf{r}_n, E)$ and the vacancy in the down (up) spin density of states $D_{\downarrow(\uparrow)}(\mathbf{r}_n, E)$, but also on the spatial overlap of the corresponding density of states. The total rate of electron-nuclear spin flip-flop now depends on the integral of $\Gamma_{\downarrow\uparrow}(\mathbf{r}_n)$ [$\Gamma_{\uparrow\downarrow}(\mathbf{r}_n)$] over the spatial coordinates:

$$\Gamma_{\uparrow\downarrow} = \frac{2\pi}{\hbar}|A_{\text{eff}}|^2 \iint d^3\mathbf{r}_n dE\, n_\uparrow(\mathbf{r}_n, E) p_\downarrow(\mathbf{r}_n, E),$$

$$\Gamma_{\downarrow\uparrow} = \frac{2\pi}{\hbar}|A_{\text{eff}}|^2 \iint d^3\mathbf{r}_n dE\, n_\downarrow(\mathbf{r}_n, E) p_\uparrow(\mathbf{r}_n, E). \quad (6)$$

The spatial dynamics of the nuclear spins can be described by the following master equation:

$$\frac{d[F(\mathbf{r}_n)]}{dt} = [\Gamma(\mathbf{r}_n)][F(\mathbf{r}_n)] - \frac{[F(\mathbf{r}_n) - F^0]}{\tau_I} + D_n\nabla^2[F(\mathbf{r}_n)], \quad (7)$$

where $[F(\mathbf{r}_n)]$ is the probability column vector representing the probability of occupancy of the nuclear spin levels, and τ_I is a phenomenological nuclear spin relaxation time, which is typically a very slow process. The matrix $\Gamma(\mathbf{r}_n)$ takes into account the transition between the individual nuclear spin levels. The vector $[F^0]$ denotes the probability of occupation of the nuclear spin levels in equilibrium. The above equation also includes nuclear spin diffusion described by the last term, where D_n is the phenomenological diffusion constant. In this paper, we neglect the exact spatial distribution of nuclear spins due to diffusion and approximate the effects of nuclear spin diffusion by incorporating a larger number of nuclei. The equation governing the dynamics of the nuclear spins is then given by

$$\frac{d[F]}{dt} = [\Gamma][F] - \frac{[F - F^0]}{\tau_I}. \quad (8)$$

The transition probability matrix $[\Gamma]$ may be specifically cast for the spin-3/2 case in the current study in terms of the spin-flip rates defined in (6) as

$$[\Gamma] = \begin{bmatrix} -\Gamma_{\downarrow\uparrow} & \Gamma_{\uparrow\downarrow} & 0 & 0 \\ \Gamma_{\downarrow\uparrow} & -(\Gamma_{\downarrow\uparrow} + \Gamma_{\uparrow\downarrow}) & \Gamma_{\uparrow\downarrow} & 0 \\ 0 & \Gamma_{\downarrow\uparrow} & -(\Gamma_{\downarrow\uparrow} + \Gamma_{\uparrow\downarrow}) & \Gamma_{\uparrow\downarrow} \\ 0 & 0 & \Gamma_{\downarrow\uparrow} & -\Gamma_{\uparrow\downarrow} \end{bmatrix}, \quad (9)$$

where $\Gamma_{\uparrow\downarrow}$ and $\Gamma_{\downarrow\uparrow}$ are defined in (6). An additional constraint used to solve (8) using (9) is that of the normalization of the nuclear state probabilities, i.e., $\sum_s F_s = 1$, where F_s is the occupation probability of the nuclear density of states with spin s.

The temporal evolution of the average electronic polarization $\langle S_z \rangle$ and the average nuclear polarization $\langle I_z \rangle$ at the QPC are calculated self-consistently by solving (8) and (3) via the relations

$$\langle S_z \rangle = \frac{1}{2} \frac{n_\uparrow - n_\downarrow}{n_\uparrow + n_\downarrow},$$

$$F_I = \langle I_z \rangle = \sum_s s F_s = [s][F], \tag{10}$$

where F_s are obtained by solving the master equations. The matrix $[s] = [\frac{3}{2} \ \frac{1}{2} \ -\frac{1}{2} \ -\frac{3}{2}]$ comprises the row vector of the spin magnetic quantum numbers of the GaAs nuclei. The procedure for transport calculations follows solving (3), (8), and (10) sequentially in a self-consistent loop with the electronic transport to be described now.

B. Electronic edge-state transport in the QPC region

While the dynamics of the nuclear spins simply follow the master equation (8) described above, a description of electronic transport involves transport currents due to the source and drain reservoirs held at electrochemical potentials μ_S and μ_D, respectively. From a Landauer-Büttiker perspective, a consistent description of transport currents in our case demands the use of both (a) direct transmission and (b) spin-flip transmission. The need to include spin-flip transmission follows from the interaction between the edge channels of different spins that gives rise to nuclear polarization which in close proximity of the QPC region determines the electronic transport. Near the QPC, the forward propagating edge channels and the backward propagating edge channels come in close proximity and hence spin-flip scattering can occur to the forward propagating as well as to the backward propagating edge channels [3].

The Landauer direct transmission $T_{\uparrow(\downarrow)}(E)$ denotes the tunneling probability of the up (down)-spin electrons through the QPC. We model the spin-split edge states in the device by a continuum of density of states as in a ballistic $1-D$ conductor [34–37] with the region of the QPC being represented by a Gaussian potential barrier, as shown in Figs. 2(a) and 2(b) along with the model used for simulation of electronic transport shown in Fig. 2(c). The direct transmission coefficients $T_\uparrow(E)$ and $T_\downarrow(E)$ are then calculated using the nonequilibrium Green's function (NEGF) method applied to the barrier described above using a $1-D$ atomistic tight-binding Hamiltonian [38,39]. The pertinent details of the approach used here have been briefly discussed in Appendix B. In our scheme, we only consider the number of transmitted modes and the filling factor at the QPC for the electronic transport which is related to the geometry of the setup that is ascertained *a priori*. Near the vicinity of $\nu_{QPC} = 1$ at the QPC, the down-spin edge channel at the QPC is almost empty in the energy range between μ_S and μ_D, resulting in a considerable simplification of the transport equations.
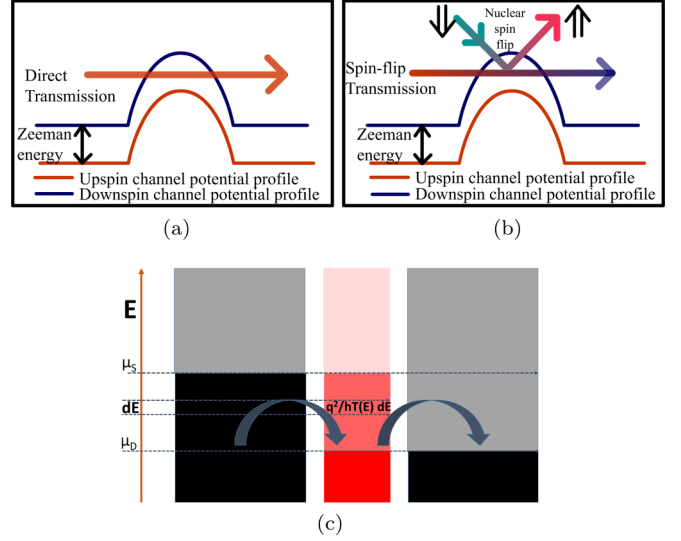

FIG. 2. Schematic of electrons tunneling through a QPC. (a) Direct transmission without spin-flip processes. The up-spin electrons are more likely to be transmitted than the down-spin electrons as a result of Zeeman splitting. (b) Electrons can suffer a spin-flip process around the QPC and transmit from the up-spin channel originating in the source contact to the down-spin channel terminating in the drain contact. (c) Schematic of the model used to simulate a single QPC structure.

We begin with the case where the filling factor $\nu_{QPC} < 1$, i.e., $G < \frac{e^2}{h}$, where only the up-spin edge channel originating from the source contact contributes to the total current terminating in the drain contact. The electrons in the forward propagating up-spin edge channel originating from the source contact can tunnel through the QPC to the up-spin edge channel terminating in the drain contact with a probability $T_\uparrow(E)$ while the forward propagating down-spin edge channel originating in the source contact is completely disconnected from the forward propagating down-spin edge channel terminating in the drain contact, as depicted in Figs. 2(a) and 2(b), respectively.

A few up-spin electrons at the QPC in the forward propagating edge channel terminating in the drain contact can however scatter to the forward propagating down-spin edge channel terminating in the drain contact with a spin-flip process as shown in Fig. 3(a). This gives rise to the spin-flip scattering current $I^{sf}_{\uparrow\downarrow(\downarrow\uparrow)}$, where the superscript "sf" denotes the flow of current due to spin-flip scattering at the QPC and the subscript '$\uparrow\downarrow(\downarrow\uparrow)$' denotes the current flow from the up (down)-spin to down (up)-spin edge channel via electronic spin-flips. Assuming that the direct transmission coefficients ($T_\uparrow$ and $T_\downarrow$) depend on the nuclear polarization only via the Overhauser field (3), for a system with four nuclear spin levels, the spin-flip transmission coefficient at the QPC from the forward propagating up-spin channel terminating in the drain contact to the forward propagating down-spin channel terminating in the drain contact is given by (details given in Appendix A)

$$T^{sff}_{\uparrow\downarrow}(E) = T_\uparrow(E) T^f_{\uparrow\downarrow} \{1 - F_{+\frac{3}{2}}\}.$$

Note that $T^f_{\uparrow\downarrow}$ depends on the spatial overlap of the density of states of the up-spin and down-spin edge channel at the
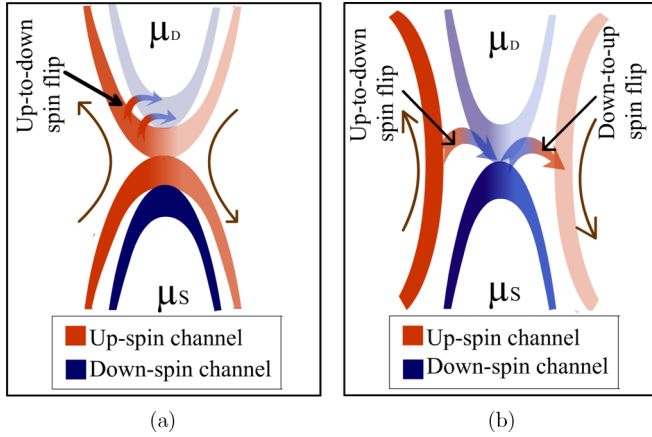
FIG. 3. Scattering schematics. (a) Associated scattering phenomena for $dI/dV < \frac{e^2}{h}(\nu_{QPC} < 1)$. Electron-nuclear spin flip-flop scattering at the QPC occurs from a forward propagating up-spin channel terminating in the drain contact to a forward propagating down-spin channel terminating in the drain contact. (b) Associated scattering phenomena for $dI/dV > \frac{e^2}{h}\nu_{QPC} > 1$. Electron-nuclear flip-flop scattering at the QPC occurs from forward propagating up-spin channel terminating in the drain contact to the forward propagating up-spin channel terminating in the drain contact and also from forward propagating down-spin channel terminating in the drain contact to the backward propagating up-spin channel originating at the drain contact. The later spin-flip scattering process decreases the conductance dI/dV because the scattering occurs to a backward propagating edge channel. A darker color in (a) and (b) indicates filled channel, while a lighter color indicates an empty channel. The up-spin and down-spin channels in (a) and (b) are indicated by brown and blue color, respectively.

QPC between the energy range μ_S and μ_D [details given in Appendix A, Eqs. (A5) and (A10)]. We approximate $T^f_{\uparrow\downarrow}$ as a constant. Therefore the down-spin current recorded just outside the QPC relies entirely on such spin-flip processes and hence is simply the spin-flip current $I^{sf}_{\uparrow\downarrow}$, while the up-spin current in the edge channel just outside the QPC is reduced by $I^{sf}_{\uparrow\downarrow}$. Based on the above discussions, the up and down spin channel currents are given by

$$I = \int dE\big(I_\uparrow(E) + I_\downarrow(E)\big)$$
$$= \frac{q}{h}\int dE\{[T_\uparrow(E) - T^{sff}_{\uparrow\downarrow}(E)] + T^{sff}_{\uparrow\downarrow}(E)\}$$
$$\times [f_S(E) - f_D(E)]. \quad (11)$$

The subscripts "S" and "D" the source and drain contacts respectively, with $f_{S(D)}(E)$ denoting the Fermi-Dirac distribution in the source (drain) contact held in quasiequilibrium at $\mu_{S(D)}$. The parameter $T^{sff}_{\uparrow\downarrow}(E)$ takes into account the spin-flip scattering of electrons at and around the QPC from the forward propagating up-spin edge channel terminating in the drain contact to the forward propagating down-spin channel terminating in the drain contact, with the superscript "sff" denoting spin-flip scattering to a forward propagating channel. It must be noted that the edge channels in the quantum Hall arrangement are uni-directional and hence the expressions

for the current in (11) depend on the factors $f_S(E)$ and $f_D(E)$ only and not on the factors $f_S(E)[1 - f_D(E)]$ and $f_D(E)[1 - f_S(E)]$ as expected in a typical Landauer type scattering treatment.

Turning our attention to the case when the filling factor $\nu_{QPC} > 1$, i.e., $G > \frac{e^2}{h}$, the down-spin electrons in the edge channel originating in the source contact are partially transmitted through the QPC to the down-spin edge channel terminating in the drain contact, as depicted in Fig. 3(b). In this case, the spin-flip scattering at and around the QPC can occur from the forward propagating up-spin channel terminating in the drain contact to the forward propagating down-spin channel terminating in the drain contact as well as from the forward propagating down-spin channel terminating in the drain contact to the backward propagating up-spin channel originating from the drain contact. Again, assuming that the direct transmission coefficients $T_\uparrow$ and $T_\downarrow$ depend on the nuclear polarization only via the Overhauser field (3), the spin-flip currents in this case are given by (details in Appendix A)

$$I^{sf}_{\uparrow\downarrow} \approx \frac{q}{h}\int dE\, T^{sff}_{\uparrow\downarrow}(E)(f_S(E) - f_D(E)),$$

$$I^{sf}_{\downarrow\uparrow} \approx \frac{q}{h}\int dE\, T^{sfb}_{\downarrow\uparrow}(E)(f_S(E) - f_D(E)),$$

where superscript "sfb" denote spin-flip scattering to a backward propagating edge channel while the superscript "sff" has the same meaning as described previously. The spin-flip current $I^{sf}_{\uparrow\downarrow}$ flows from the forward propagating up-spin channel terminating in the drain contact to the forward propagating down-spin edge channel terminating in the drain contact while the spin-flip current $I^{sf}_{\downarrow\uparrow}$ flows from the forward propagating down-spin edge channel terminating in the drain contact to the backward propagating up-spin channel originating in the drain contact. Hence $I^{sf}_{\downarrow\uparrow}$ causes a change in the total output current since the spin-flip scattering occurs to a backward propagating edge channel. It, however, does play a role in the nuclei polarization near the QPC. The current in the up-spin and down-spin channel terminating in the drain contact just outside the QPC is then given by

$$I_\uparrow = \int \frac{q}{h}[T_\uparrow(E) - T^{sff}_{\uparrow\downarrow}(E)][f_S(E) - f_D(E)]dE$$
$$= \int \frac{q}{h}[T_\uparrow(E) - T_\uparrow(E)T^f_{\uparrow\downarrow}(1 - F_{\frac{3}{2}})]$$
$$\times [f_S(E) - f_D(E)]dE, \quad (12)$$

$$I_\downarrow = \int \frac{q}{h}[T_\downarrow(E) + T^{sff}_{\uparrow\downarrow}(E) - T^{sfb}_{\downarrow\uparrow}(E)][f_S(E) - f_D(E)]dE$$
$$= \int \frac{q}{h}[T_\downarrow(E) + T_\uparrow(E)T^f_{\uparrow\downarrow}(1 - F_{\frac{3}{2}})$$
$$- T_\downarrow(E)T^b_{\downarrow\uparrow}(1 - F_{-\frac{3}{2}})][f_S(E) - f_D(E)]dE. \quad (13)$$

From the above discussion, the generalized equations for the up-spin, down-spin and spin-flip currents through the QPC are

given by

$$I_\uparrow = \frac{q}{h} \int \left\{ \underbrace{T_\uparrow(E)}_{\substack{Direct \\ Transmission}} + \underbrace{T_{\downarrow\uparrow}^{sff}(E) - T_{\uparrow\downarrow}^{sff}(E)}_{\substack{spin-flip \\ forward-transmission}} - \underbrace{T_{\uparrow\downarrow}^{sfb}(E)}_{\substack{spin-flip \\ backward-transmission}} \right\} \times \{f_S(E) - f_D(E)\}dE$$

$$= \frac{q}{h} \int \left\{ T_\uparrow(E) + T_{\downarrow\uparrow}^f T_\downarrow(E)\{1 - F_{-\frac{3}{2}}\} - T_{\uparrow\downarrow}^f T_\uparrow(E)\{1 - F_{\frac{3}{2}}\} - T_{\uparrow\downarrow}^b T_\uparrow(E)\{1 - F_{\frac{3}{2}}\} \right\} \times \{f_S(E) - f_D(E)\}dE$$

$$I_\downarrow = \frac{q}{h} \int \left\{ \underbrace{T_\downarrow(E)}_{\substack{Direct \\ Transmission}} + \underbrace{T_{\uparrow\downarrow}^{sff}(E) - T_{\downarrow\uparrow}^{sff}(E)}_{\substack{spin-flip \\ forward-transmission}} - \underbrace{T_{\downarrow\uparrow}^{sfb}(E)}_{\substack{spin-flip \\ backward-transmission}} \right\} \times \{f_S(E) - f_D(E)\}dE$$

$$= \frac{q}{h} \int \left\{ T_\downarrow(E) + T_{\uparrow\downarrow}^f T_\uparrow(E)\{1 - F_{\frac{3}{2}}\} - T_{\downarrow\uparrow}^f T_\downarrow(E)\{1 - F_{-\frac{3}{2}}\} - T_{\downarrow\uparrow}^b T_\downarrow(E)\{1 - F_{-\frac{3}{2}}\} \right\} \times \{f_S(E) - f_D(E)\}dE$$

$$I^{sf} = |I_{\uparrow\downarrow}^{sf}| - |I_{\downarrow\uparrow}^{sf}|$$

$$= \frac{q}{h} \int \{T_{\uparrow\downarrow}^{sff}(E) + T_{\uparrow\downarrow}^{sfb}(E) - T_{\downarrow\uparrow}^{sff}(E) - T_{\downarrow\uparrow}^{sfb}(E)\} \times \{f_S(E) - f_D(E)\}dE \tag{14}$$

where $T_\uparrow(E)$ and $T_\downarrow(E)$ are the direct transmission coefficients between the forward propagating edge channels originating and terminating in the source and drain contacts respectively through the QPC in the absence of electron-nuclear spin flip-flop scattering. As already discussed, the terms $T_{\downarrow\uparrow}^{sff}(E)$ and $T_{\uparrow\downarrow}^{sff}(E)$ characterize spin-flip scattering from a forward propagating edge channel terminating in the drain contact to a forward propagating edge channel terminating in the drain contact at the QPC, while $T_{\uparrow\downarrow}^{sfb}(E)$ and $T_{\downarrow\uparrow}^{sfb}(E)$ characterize spin-flip scattering at the QPC from a forward propagating edge state terminating in the drain contact to a backward propagating edge channel originating in the drain contact at the QPC. The terms $T_{\downarrow\uparrow}^{sff}(E)$, $T_{\uparrow\downarrow}^{sff}(E)$, $T_{\uparrow\downarrow}^{sfb}(E)$, and $T_{\downarrow\uparrow}^{sfb}(E)$, being the probability of electron-nuclear spin flip-flop processes, are dependent on the nuclear polarization (details given in Appendix A). The spin-flip currents $I_{\uparrow\downarrow}^{sf}$ and $I_{\downarrow\uparrow}^{sf}$ give rise to nuclear polarization at and around the QPC region.

Turning our attention to the self-consistent solution of the electronic transport and the temporal evolution of the nuclear polarization, the electronic transport is influenced by the nuclear polarization via the Overhauser field while the evolution of nuclear polarization is determined by the spin-flip current and the nuclear spin-lattice relaxation time (τ_I). The matrix $[\Gamma]$, which determines the temporal evolution in nuclear polarization is hence related to the spin-flip currents $I_{\uparrow\downarrow}^{sf}$ and $I_{\downarrow\uparrow}^{sf}$. A schematic diagram on self-consistency involved in the temporal evolution of nuclear polarization and electronic transport phenomena is shown in Fig. 4. For a system with quad nuclear spin levels as in GaAs, it can be shown that $\Gamma_{\downarrow\uparrow} = C_2|I_{\downarrow\uparrow}^{sf}|$ and $\Gamma_{\uparrow\downarrow} = C_1|I_{\uparrow\downarrow}^{sf}|$ with $C_1 = \frac{1}{qN_I\{1-F_{\frac{3}{2}}\}}$ and $C_2 = \frac{1}{qN_I\{1-F_{-\frac{3}{2}}\}}$ (details given in Appendix C), N_I being the number of nuclei that are being influenced by spin flip-flop processes at the QPC. We can hence rewrite the expression for $[\Gamma]$ as (details given in Appendix C):

$$[\Gamma] = \begin{bmatrix} -C_2|I_{\downarrow\uparrow}^{sf}| & C_1|I_{\uparrow\downarrow}^{sf}| & 0 & 0 \\ C_2|I_{\downarrow\uparrow}^{sf}| & -(C_2|I_{\downarrow\uparrow}^{sf}| + C_1|I_{\uparrow\downarrow}^{sf}|) & C_1|I_{\uparrow\downarrow}^{sf}| & 0 \\ 0 & C_2|I_{\downarrow\uparrow}^{sf}| & -(C_2|I_{\downarrow\uparrow}^{sf}| + C_1|I_{\uparrow\downarrow}^{sf}|) & C_1|I_{\uparrow\downarrow}^{sf}| \\ 0 & 0 & C_2|I_{\downarrow\uparrow}^{sf}| & -C_1|I_{\uparrow\downarrow}^{sf}| \end{bmatrix}. \tag{15}$$

Let us now consider the experimental features on a case by case basis.

III. RESULTS

A. Conductance hysteresis with voltage sweep

We first reproduce some trends noted in the conductance plots of a recent experiment [3] where a change in the conductance along with hysteresis in the conductance was noted in the vicinity of $V = 0$ with a positive and a negative

source to drain voltage sweep. We explain the possible phenomena giving rise to such experimental trends.

1. Case I: $dI/dV < e^2/h$

A schematic of the scattering processes in this regime is shown in Fig. 3(a), while the up-spin and down-spin edge current paths and equivalent circuit models for the phenomena occurring around the QPC are shown in Figs. 5(a) and 5(b), respectively. In this case, the following points are to be noted. (1) Only the up-spin channel is transmitted through the QPC.

Electronic transport

$$U_\uparrow(z) = U_O - \frac{g\mu_B B}{2} + \frac{A_{eff}F_I}{2}$$

$$U_\downarrow(z) = U_O + \frac{g\mu_B B}{2} - \frac{A_{eff}F_I}{2}$$

Compute $T_\uparrow$, $T_\downarrow$, $T_{\uparrow\downarrow}^{sf}$, $T_{\downarrow\uparrow}^{sf}$

Compute $I_\uparrow$, $I_\downarrow$, $I_{\uparrow\downarrow}^{sf}$, $I_{\downarrow\uparrow}^{sf}$

$I_{\uparrow\downarrow}^{sf}, I_{\downarrow\uparrow}^{sf}$
$(Eq.\ 3, 14, A10, A11)$

F_I, F
$(Eq.\ 8, 9, 10)$

Nuclear spin dynamics

$$\frac{d[F(\xi)]}{dt} = \left[\frac{d[F(\xi)]}{dt}\right]_{flip-flop} + \left[\frac{d[F(\xi)]}{dt}\right]_{relaxation} + \left[\frac{d[F(\xi)]}{dt}\right]_{NMR}$$

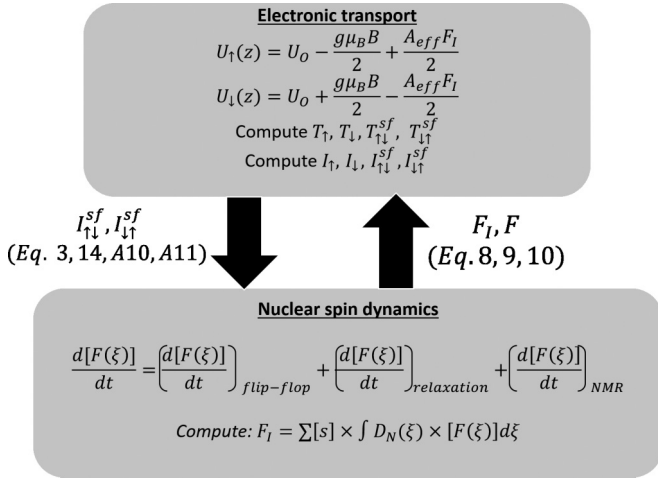Compute: $F_I = \sum[s] \times \int D_N(\xi) \times [F(\xi)]d\xi$

FIG. 4. Schematic diagram showing the self-consistency involved in solving the electron transport dynamics and the nuclear spin dynamics in time domain.

(2) The down-spin channel originating in the source contact is totally reflected at the QPC. (3) Some up-spin electrons in the edge channel terminating in the drain contact can scatter at the QPC to the down-spin edge channel terminating in the drain contact via electron-nuclear spin flip-flop scattering. Such a scattering decreases the current in the up-spin channel just outside the QPC and increases the current in the down-spin edge channel outside the QPC. However, the total current remains proportional to $T_\uparrow(E)$.

We believe that the reasons for an increase in dI/dV near $V = 0$ are the following. (1) Near $V = 0$, the nuclear polarization cannot be maintained. (2) Nuclear polarization drops due to spin lattice relaxation. (3) A drop in nuclear polarization results in an increase in the direct transmission coefficient $T_\uparrow$ of the up-spin channel due to a decrease in the Overhauser field as well as an increase in the spin-flip transmission coefficient $T_{\uparrow\downarrow}^{sff}$.

A schematic of the edge channel path in this case is shown in Fig. 5(a), while the equivalent circuit in this case is detailed in Fig. 5(b) to aid a visualization of the various transport phenomena inside the device. The circuit model can be described as follows. (1) The up-spin edge channel is represented by a conductance $G = 0.68\frac{e^2}{h}$. (2)The up-to-down spin-flip scattering can be represented by an equivalent current source from the up-spin channel. $I_{UD} = 0.01I_U[1 - F_{\frac{3}{2}}]$. (3) The change in transmissivity of the up-spin channel due to
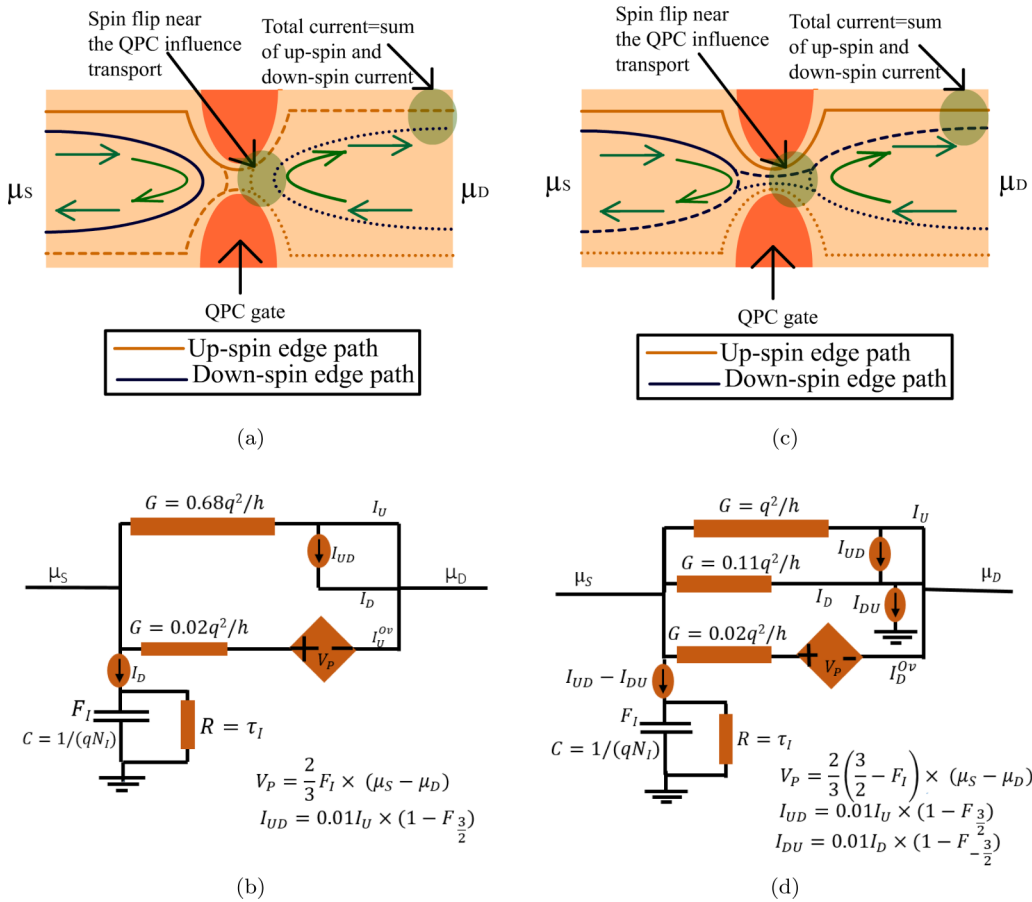

Spin flip near the QPC influence transport

Total current=sum of up-spin and down-spin current

μ_S μ_D

QPC gate

—— Up-spin edge path
—— Down-spin edge path

(a)

Spin flip near the QPC influence transport

Total current=sum of up-spin and down-spin current

μ_S μ_D

QPC gate

—— Up-spin edge path
—— Down-spin edge path

(c)

$G = 0.68q^2/h$ I_U

μ_S I_{UD} μ_D

I_D

$G = 0.02q^2/h$ I_U^{Ov}

$+ V_P -$

I_D

F_I

$C = 1/(qN_I)$ $R = \tau_I$

$$V_P = \frac{2}{3}F_I \times (\mu_S - \mu_D)$$

$$I_{UD} = 0.01I_U \times (1 - F_{\frac{3}{2}})$$

(b)

$G = q^2/h$ I_U

$G = 0.11q^2/h$ I_{UD}

μ_S I_D I_{DU} μ_D

$G = 0.02q^2/h$

$I_{UD} - I_{DU}$ $+ V_P -$ I_D^{Ov}

F_I

$C = 1/(qN_I)$ $R = \tau_I$

$$V_P = \frac{2}{3}\left(\frac{3}{2} - F_I\right) \times (\mu_S - \mu_D)$$

$$I_{UD} = 0.01I_U \times (1 - F_{\frac{3}{2}})$$

$$I_{DU} = 0.01I_D \times (1 - F_{-\frac{3}{2}})$$

(d)

FIG. 5. Schematic of current path and equivalent circuit models. (a) Associated up-spin and down-spin current path for $dI/dV < \frac{e^2}{h}(\nu_{QPC} < 1)$. (b) Equivalent lumped circuit diagram for (a). (c) Associated up-spin and down-spin current path for $dI/dV > \frac{e^2}{h}(\nu_{QPC} > 1)$. (d) Equivalent lumped circuit diagram for (c). The up-spin and down-spin channels in figure (a) and (c) are indicated by brown and blue color, respectively. In the energy range between μ_S and μ_D, the filled, partially filled, end empty edge states are denoted by solid line, dashed lines, and dotted lines, respectively.

the Overhauser field is represented by a by an equivalent conductor ($G = 0.02\frac{e^2}{h}$) in series with a voltage dependent voltage source $V_p = \frac{2}{3}F_I\,[\mu_S - \mu_D]$. The current change due to the Overhauser field is represented by I_U^{Ov}. (4) The nuclear polarization is represented by the voltage across the capacitor. (5) The resistance in parallel with the capacitor represents nuclear spin-lattice relaxation.

2. Case II $dI/dV > e^2/h$

A schematic of the scattering processes in this regime is shown in Fig. 3(b), while the up-spin and down-spin edge current paths and equivalent circuit models for the phenomena occurring around the QPC are shown in Figs. 5(c) and 5(d), respectively. In this case, the following points are to be noted. (1) The up-spin electrons in the edge channel originating in the source contact are fully transmitted through the QPC to the up-spin edge channel terminating in the drain contact. (2) The down-spin electrons in the edge channel originating in the source contact are partially transmitted through the QPC to the down-spin edge channel terminating in the drain contact. (3) Two kinds of electron-nuclear spin-flip scattering dominate at the QPC in this case: (i) electrons from the forward propagating up-spin channel terminating in the drain contact can undergo spin-flip scattering to the forward propagating down-spin channel terminating in the drain contact, which is almost empty in the energy range between μ_S and μ_D. Such scattering at and around the QPC results in a positive nuclear polarization. (ii) Electrons in forward propagating down-spin channel propagating through the QPC can undergo a spin-flip scattering to the backward propagating up-spin channel (which is totally empty in the energy range between μ_S and μ_D) terminating in the source contact. Such scattering results in a negative nuclear polarization in addition to decreasing the total current through the QPC. (4) Out of these two processes, the former process dominates at the QPC due to the presence of more up-spin electrons compared to down-spin electrons resulting in a net positive nuclear polarization at the QPC.

We believe that the reasons for a decrease in dI/dV near $V = 0$ are the following. (1) Near $V = 0$, the nuclear polarization cannot be maintained. (2) Nuclear polarization drops due to spin-lattice relaxation. (3) A drop in polarization results in an increase in the up-to-down spin-flip rate as well as a decrease in down-to-up spin-flip rate in addition to a decrease in the direct transmission coefficient $T_\downarrow$ of the down-spin channel due to decrease in the Overhauser field. (4) The decrease in transmission coefficient of the down-spin channel decreases the conductance of the QPC in the vicinity of $V = 0$.

The equivalent circuit in this case is detailed in Fig. 5(d). The circuit model can be described as follows. (1) The up-spin edge channel originating in the source contact is fully transmitted through the QPC and hence is represented by a conductance $G = e^2/h$. (2) The down-spin edge channel originating in the source contact is partially transmitted through the QPC to the down-spin edge channel terminating in the drain contact and hence is represented by a conductance $G = 0.11\frac{e^2}{h}$. (3) The up-to-down spin-flip current at the QPC from the forward propagating up-spin channel terminating in the drain contact to the forward propagating down-spin
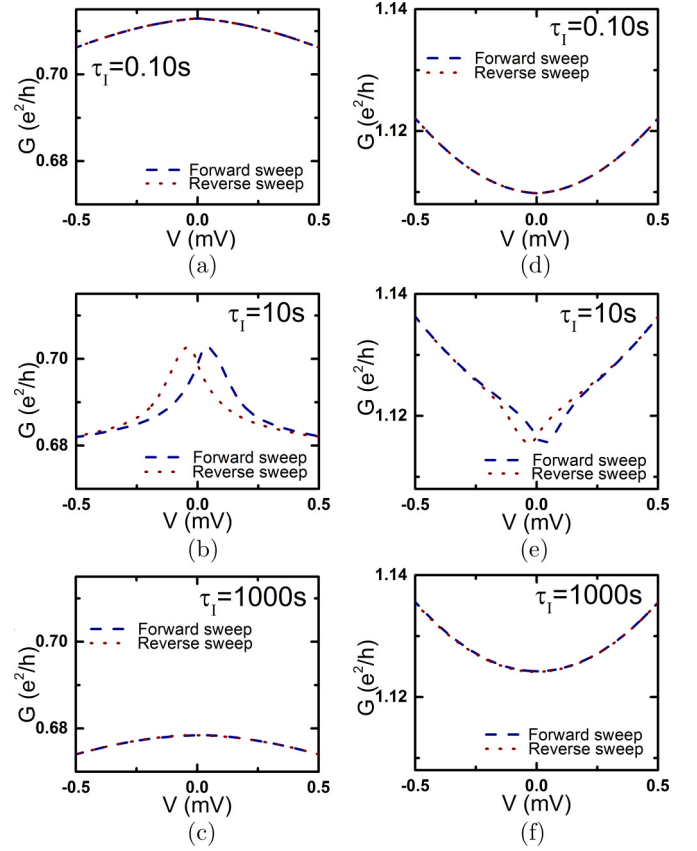

FIG. 6. Simulated plots of conductance-voltage ($G - V$) traces during a voltage sweep. Left panel (a,b,c): for the case $G < \frac{e^2}{h}$, Right panel (d,e,f): for the case $G > \frac{e^2}{h}$, Top panel (a,d): the case when $\tau_I = 0.1$ s, Middle panel (b,e): the case when $\tau_I = 10$ s, Bottom panel (c,f): the case when $\tau_I = 1000$ s. The parameters used in the simulations are: $B = 4T$, $N_I = 10^9$, $T_{\uparrow\downarrow}^f = 0.01$, $T_{\downarrow\uparrow}^f = 0$, $T_{\uparrow\downarrow}^b = 0$, $T_{\downarrow\uparrow}^b = 0.01$. Total sweep time $= 200$ s.

channel terminating in the drain contact is represented by a current dependent current source $I_{UD} = 0.01I_U\,[1 - F_{\frac{3}{2}}]$. (4) The down-to-up spin-flip current from the forward propagating down-spin channel originating in the source contact to the backward propagating up-spin channel terminating in the source contact is represented by a current-dependent current source $I_{DU} = 0.01I_D\,[1 - F_{-\frac{3}{2}}]$. (5) The change in the transmission coefficient of the down-spin channel due to the Overhauser field is represented by a by an equivalent conductor ($G = 0.02\frac{e^2}{h}$) in series with a voltage dependent voltage source ($V_p = \frac{2}{3}[\frac{3}{2} - F_I]\,[\mu_S - \mu_D]$). The current change due to the Overhauser field is represented by I_D^{Ov}. (6) The nuclear polarization is represented by the voltage across the capacitor. (7) The resistance in parallel with the capacitor represents nuclear spin-lattice relaxation by causing charge leakage from the capacitor.

The simulated results of the change in conductance with source to drain voltage sweeps are shown in Fig. 6. The parameters $T_\uparrow$ and $T_\downarrow$ in the simulations are calculated directly via a $1 - D$ nonequilibrium Green's function (NEGF) method using an atomistic tight-binding Hamiltonian [38–40] while the parameters $T_{\uparrow\downarrow}^{sff}$ and $T_{\downarrow\uparrow}^{sfb}$ are calculated using (A10). The

parameters in the above illustration for the circuit diagrams in Fig. 3 are chosen to match the simulated result of the change in conductance with source to drain voltage sweep. The maximum change in the conductance due to a difference in the Overhauser field between the fully polarized nuclei and the nonpolarized nuclei is less than $G_{Ov} = 0.02\frac{e^2}{h}$. However, this maximum change can be enhanced due to spin flip-flop tunneling as noted experimentally [3]. The hysteresis in the G-V curves in Fig. 6 near $V = 0$ occurs only when the nuclear spin relaxation time (τ_I) is of the order of the voltage sweep time. This results in a lag between the applied voltage and nuclear polarization near $V = 0$ thereby resulting in the hysteresis. The hysteresis in G-V plots disappear when the τ_I is very large such that the change in nuclear polarization is negligible during the time of voltage sweep. The hysteresis in G versus V plots also disappear when τ_I is very small compared to the voltage sweep time because the nuclear polarization is always in a steady state with the applied voltage.

B. Resistively detected nuclear magnetic resonance (RDNMR)

We begin our analysis with (14), where the nuclear polarization in the vicinity of the QPC is perturbed by an externally applied alternating magnetic field in the radio-frequency (RF) range resulting in the Zeeman split nuclear levels to interact with each other. Near the frequency corresponding to the difference in energy between the two spin split nuclear energy levels ($\hbar\omega = \xi_{s+1} - \xi_s$), precession of the nuclear spins accompanied by a rapid decay in the nuclear polarization occurs.

To model such processes, we model the spin split nuclear energy levels by a broadened normalized density of states [30,38,39]:

$$D_s(\xi) = \frac{1}{2\pi}\frac{\eta}{(\xi - \epsilon_s)^2 + (\frac{\eta}{2})^2},$$

where ξ is the free variable denoting energy in the nuclear spin space, η is related to the amount of broadening of the nuclear spin levels and ϵ_s is the energy level of the sth nuclear spin in the absence of broadening. Broadening might be a result of thermal motion of the nucleus [30], hyperfine interaction mediated electron-nuclear spin exchange [30] as well as nuclear dipole-dipole exchange interaction [30], which is the causative agent for nuclear spin diffusion [30]. We take broadening to be $\eta = 10^{-4}$ μeV. We simulate the case of quad nuclear spin levels, as in GaAs, separated in energy due to Zeeman splitting. The rate equations in this case are given by

$$\left[\frac{dF(\xi)}{dt}\right] = \left[\frac{dF(\xi)}{dt}\right]_{\text{flip-flop}} + \left[\frac{dF(\xi)}{dt}\right]_{\text{relaxation}}$$
$$+ \left[\frac{dF(\xi)}{dt}\right]_{\text{NMR}}, \quad (16)$$

$$F_I = \int_{-\infty}^{\infty} [s] \times [D_N(\xi)] \times [F(\xi)]d\xi, \quad (17)$$

$$T_{\downarrow\uparrow}^{sff}(E) = T_{\downarrow\uparrow}^f T_\downarrow(E)\left[1 - \int D_{-\frac{3}{2}}(\xi)F_{-\frac{3}{2}}(\xi)d\xi\right],$$

$$T_{\uparrow\downarrow}^{sff}(E) = T_{\uparrow\downarrow}^f T_\uparrow(E)\left[1 - \int D_{\frac{3}{2}}(\xi)F_{\frac{3}{2}}(\xi)d\xi\right],$$

$$T_{\downarrow\uparrow}^{sfb}(E) = T_{\downarrow\uparrow}^b T_\downarrow(E)\left[1 - \int D_{-\frac{3}{2}}(\xi)F_{-\frac{3}{2}}(\xi)d\xi\right],$$

$$T_{\uparrow\downarrow}^{sfb}(E) = T_{\uparrow\downarrow}^b T_\uparrow(E)\left[1 - \int D_{\frac{3}{2}}(\xi)F_{\frac{3}{2}}(\xi)d\xi\right], \quad (18)$$

$$I_{\uparrow\downarrow}^{sf} = \int \frac{e}{h}[T_{\uparrow\downarrow}^{sff}(E) + T_{\uparrow\downarrow}^{sfb}(E)][f_S(E) - f_D(E)]dE,$$

$$I_{\downarrow\uparrow}^{sf} = \int \frac{e}{h}[T_{\downarrow\uparrow}^{sff}(E) + T_{\downarrow\uparrow}^{sfb}(E)][f_S(E) - f_D(E)]dE, \quad (19)$$

where $[s] = [\frac{3}{2}\ \frac{1}{2}\ -\frac{1}{2}\ -\frac{3}{2}]$ is the row vector denoting four nuclear spin levels in GaAs and $[F(\xi)] = [F_{\frac{3}{2}}(\xi)\ F_{\frac{1}{2}}(\xi)\ F_{-\frac{1}{2}}(\xi)\ F_{-\frac{3}{2}}(\xi)]^\dagger$. $F_s(\xi)$ is the probability of occupancy of the density of states of the sth nuclear spin level D_s at energy ξ. The matrix $D_N(\xi)$ is the diagonal matrix representing the nuclear density of states at energy ξ given by

$$D_N(\xi) = \begin{bmatrix} D_{\frac{3}{2}}(\xi) & 0 & 0 & 0 \\ 0 & D_{\frac{1}{2}}(\xi) & 0 & 0 \\ 0 & 0 & D_{-\frac{1}{2}}(\xi) & 0 \\ 0 & 0 & 0 & D_{-\frac{3}{2}}(\xi) \end{bmatrix}.$$

At low temperatures, $\{f_S(E) - f_D(E)\}$ is a boxcar function. Assuming that the average value of $T_\uparrow$ and $T_\downarrow$ in the energy range between μ_S and μ_D are $T_\uparrow^{\text{avg}}$ and $T_\downarrow^{\text{avg}}$, respectively, and the spin-flip transmission coefficients, $T_{\uparrow\downarrow}^{f(b)}$ and $T_{\downarrow\uparrow}^{f(b)}$, are constant in the range of energy between μ_S and μ_D, the above equation can be simplified to

$$I_{\uparrow\downarrow}^{sf} = \frac{e}{h}T_\uparrow^{\text{avg}}[T_{\uparrow\downarrow}^f + T_{\uparrow\downarrow}^b]\left[1 - \int D_{\frac{3}{2}}(\xi)F_{\frac{3}{2}}(\xi)d\xi\right]\Delta\mu$$
$$= \frac{e^2}{h}T_\uparrow^{\text{avg}}T_{\uparrow\downarrow}^{\text{avg}}\left[1 - \int D_{\frac{3}{2}}(\xi)F_{\frac{3}{2}}(\xi)d\xi\right]V,$$

$$I_{\downarrow\uparrow}^{sf} = \frac{e}{h}T_\downarrow^{\text{avg}}[T_{\downarrow\uparrow}^f + T_{\downarrow\uparrow}^b]\left[1 - \int D_{-\frac{3}{2}}(\xi)F_{-\frac{3}{2}}(\xi)d\xi\right]\Delta\mu$$
$$= \frac{e^2}{h}T_\downarrow^{\text{avg}}T_{\downarrow\uparrow}^{\text{avg}}\left[1 - \int D_{-\frac{3}{2}}(\xi)F_{-\frac{3}{2}}(\xi)d\xi\right]V, \quad (20)$$

where $\Delta\mu = \mu_S - \mu_D$. The set of equations (16)–(19) have to be solved self-consistently to calculate the temporal evolution of the nuclear polarization. If the coherence between the nuclear spins is neglected, then the rate of decay of nuclear polarization with time due to perturbation via an externally applied RF field can be characterized phenomenologically by a time constant τ_{NMR}. The rate of decay of nuclear polarization with RF frequency sweep without taking into account the correlation between nuclear spins is given by the equation

$$\left[\frac{dF(\xi)}{dt}\right]_{\text{NMR}} = \text{diag}\left(\frac{1}{\tau_{\text{NMR}}}\frac{\pi\eta}{2}[\Gamma_{\text{NMR}}(\xi)][F_{\text{NMR}}(\xi,\hbar\omega)]\right).$$

The matrix $\Gamma_{\text{NMR}}(\xi)$ takes into account the net rate of transition between consecutive nuclear spin levels depending on the energy of the RF frequency photons ($\hbar\omega$) and is given by

(details given in Appendix D)

$$\Gamma_{NMR}(\xi) = \begin{bmatrix} -D_{\frac{1}{2}}(\xi - \hbar\omega) & D_{\frac{1}{2}}(\xi - \hbar\omega) & 0 & 0 \\ D_{\frac{3}{2}}(\xi + \hbar\omega) & -[D_{\frac{3}{2}}(\xi + \hbar\omega) + D_{-\frac{1}{2}}(\xi - \hbar\omega)] & D_{-\frac{1}{2}}(\xi - \hbar\omega) & 0 \\ 0 & D_{\frac{1}{2}}(\xi + \hbar\omega) & -[D_{\frac{1}{2}}(\xi + \hbar\omega) + D_{-\frac{3}{2}}(\xi - \hbar\omega)] & D_{-\frac{3}{2}}(\xi - \hbar\omega) \\ 0 & 0 & D_{-\frac{1}{2}}(\xi + \hbar\omega) & -D_{-\frac{1}{2}}(\xi + \hbar\omega) \end{bmatrix}$$

$$F_{\text{NMR}}(\xi, \hbar\omega) = \begin{bmatrix} F_{\frac{3}{2}}(\xi) & F_{\frac{3}{2}}(\xi + \hbar\omega) & 0 & 0 \\ F_{\frac{1}{2}}(\xi - \hbar\omega) & F_{\frac{1}{2}}(\xi) & F_{\frac{1}{2}}(\xi + \hbar\omega) & 0 \\ 0 & F_{-\frac{1}{2}}(\xi - \hbar\omega) & F_{-\frac{1}{2}}(\xi) & F_{-\frac{1}{2}}(\xi + \hbar\omega) \\ 0 & 0 & F_{-\frac{3}{2}}(\xi - \hbar\omega) & F_{-\frac{3}{2}}(\xi) \end{bmatrix} \tag{21}$$

with τ_{NMR} being of the order of 100 μs [4,5]. We now present some simulation results based on the above model. Specifically, we present results for three different sweep times in Fig. 7 and show how the rate of sweep of RF frequency influence the hysteresis observed in the R_H traces.

We note that the hysteresis is a result of the slow buildup of nuclear polarization. The hysteresis disappears if the sweep
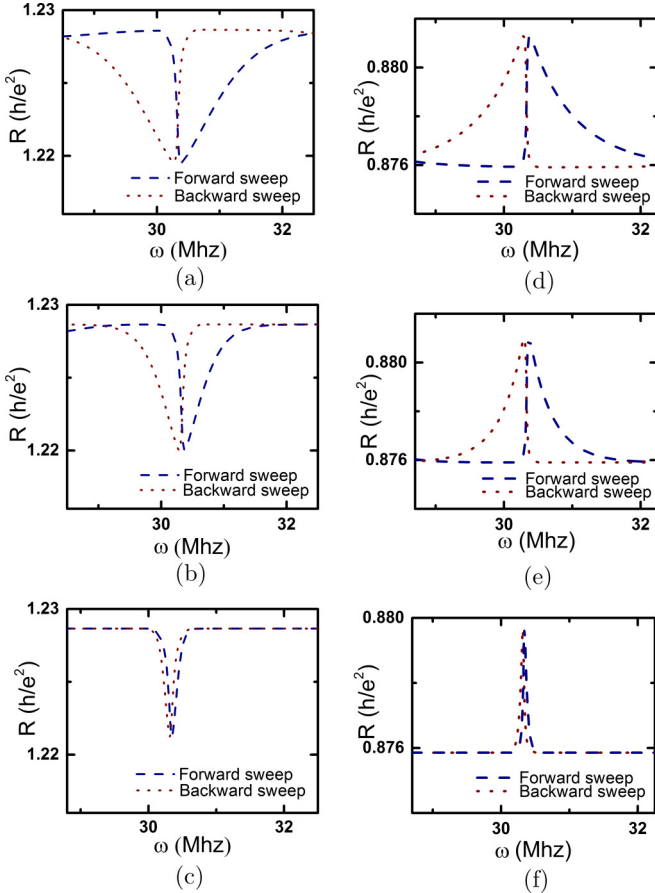

FIG. 7. Plots of resistance variation with NMR frequency sweep (RDNMR traces) at various sweep rates. Top panel: Plots for total sweep time = 50 s, Middle panel: Plots for total sweep time = 100 s, Bottom panel: Plots for total sweep time = 500 s. Left panel (a, b, c): Plots for $R > \frac{h}{e^2}$ ($\nu_{QPC} < 1$), Right panel (d, e, f): Plots for $R < \frac{h}{e^2}$ ($\nu_{QPC} > 1$). Simulations are done for $B = 4T$, $N_I = 10^9$, $T_{\uparrow\downarrow}^f = 0.01$, $T_{\uparrow\downarrow}^b = 0$, $T_{\downarrow\uparrow}^f = 0$, $T_{\downarrow\uparrow}^b = 0.01$. $T_\uparrow$ and $T_\downarrow$ are calculated using NEGF formalism as elaborated in the text.

rate is much slower compared to the rate of buildup of nuclear polarization. On the other hand, hysteresis is pronounced if the sweep rate is much faster compared to the rate of buildup of nuclear polarization. The change in conductance during NMR frequency sweep is mainly due to the effect of the Overhauser field on the transmission coefficient of the spin channels at the QPC as well as the spin-flip scattering at the QPC. For $R > \frac{h}{e^2}$ ($\nu_{QPC} < 1$), the up-spin electrons in the forward propagating edge channel terminating in the drain contact can scatter at the QPC to the forward propagating down-spin edge channel terminating in the drain contact with a spin-flip scattering. Such electron-nuclear spin flip-flop processes create a positive nuclear polarization which opposes the effect of the magnetic field on the up-spin channel by enhancing it's potential barrier at the QPC, resulting in a decrease in the transmission coefficient of the up-spin channel. Destruction of nuclear polarization via NMR frequency perturbation hence results in a decrease in the up-spin channel resistivity due to an increase in the transmission coefficient (decrease in the Overhauser field).

For $R < \frac{h}{e^2}$ ($\nu_{\text{QPC}} > 1$), the electrons in the forward propagating down-spin edge channel originating in the source contact can transmit partially to the down-spin edge channel terminating in the drain contact. The forward propagating down-spin edge channel originating in the source contact being partially transmitted through the QPC, two spin flip-flop scattering mechanism may be dominant at and around the QPC-(i) A net spin-flip scattering from the forward propagating up-spin edge channel terminating in the drain contact to the forward propagating down-spin edge channel terminating in the drain contact. Such spin-flip scattering creates positive nuclear polarization. (ii) A net spin-flip scattering from forward propagating down-spin edge channel terminating in the drain contact to backward propagating up-spin edge channel terminating in the source contact (the forward propagating up-spin channel is full). Such spin-flip scattering creates negative nuclear polarization and also decreases the total current through the QPC. At $R \approx \frac{h}{e^2} - \epsilon$, most of the electron spin flipping at the QPC occurs from the forward propagating up-spin edge channel terminating in the drain contact to the forward propagating down-spin edge channel terminating in the drain contact (since the majority of electrons at the QPC occupy the up-spin channel) which creates net positive nuclear polarization. Although positive nuclear polarization influences the transmission coefficient of both down spin and up-spin channel, the relative feedback on the up-spin channel is much

less compared to that on the down-spin channel. Positive nuclear polarization enhances the transmission coefficient of the down-spin edge channel through the QPC. Destruction of nuclear spin polarization during NMR frequency perturbation
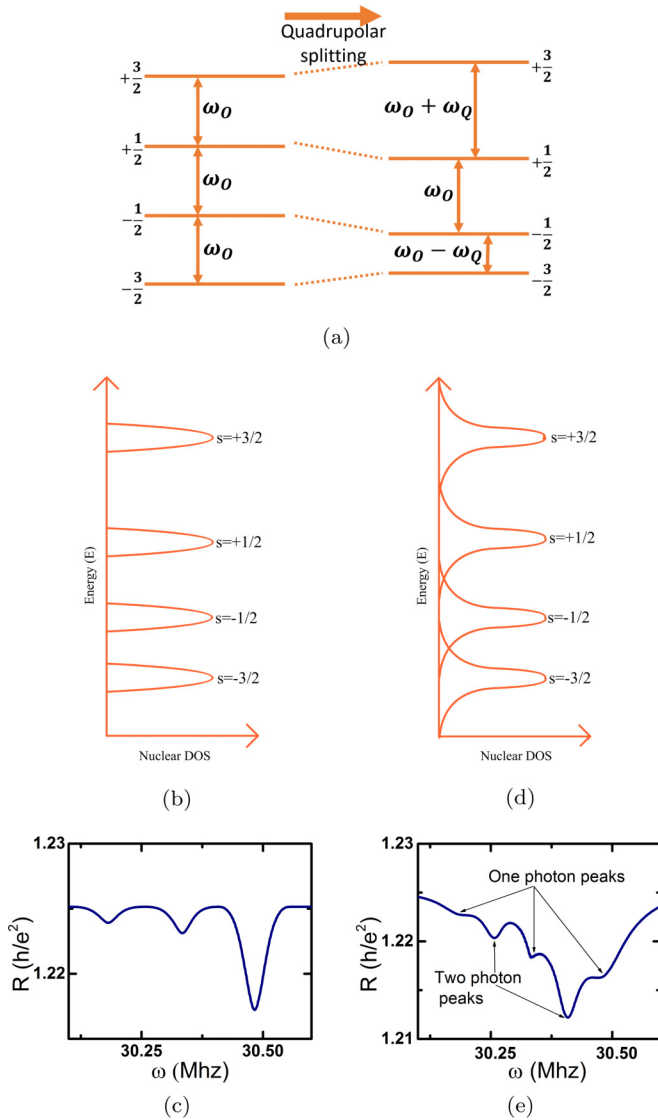

(a)

(b)

(c)

(d)

(e)

FIG. 8. Signatures of quadrupolar splitting on RDNMR traces. (a) Schematic diagram showing nuclear spin levels unevenly split due to quadrupolar splitting. (b) Schematic of broadened nuclear density of states without any intermediate state for multiphoton absorption. The density of states is truncated and of finite extent in nuclear energy space. (c) Plot showing one photon peaks in the conductance with RF frequency sweep in case of nuclear quadrupolar splitting for $R > \frac{h}{e^2}$ ($\nu_{\text{QPC}} < 1$). (d) Schematic of broadened nuclear density of states with small nuclear density of states between the peaks in the density of states to aid multiphoton transitions. (e) Plot showing single photon and multiphoton peaks in the conductance with RF frequency sweep in case of strain induced quadrupolar splitting for $R > \frac{h}{e^2}$ ($\nu_{\text{QPC}} < 1$). The two photon processes in our simulation can be accounted for by incorporating infinitesimally small nuclear density of states between the peaks of the nuclear density of states. Simulations are done for $B = 4T$, $N_I = 10^9$, $T^f_{\uparrow\downarrow} = 0.01$, $T^b_{\uparrow\downarrow} = 0$, $T^f_{\downarrow\uparrow} = 0$, $T^b_{\downarrow\uparrow} = 0.01$. $T_\uparrow$ and $T_\downarrow$ are calculated using NEGF formalism as elaborated in the text.

hence results in an increase in the resistivity of the down-spin edge channel due to decrease in transmission coefficient of the down-spin channel through the QPC. The plots of the Hall resistance versus the RF frequency sweep for the two cases (a) $R > \frac{h}{e^2}$ ($\nu_{\text{QPC}} < 1$) and (b) $R < \frac{h}{e^2}$ ($\nu_{\text{QPC}} > 1$) are shown in Fig. 7.

C. Capturing quadrupolar peaks

A current focus area in quantum computing is the possibility of information processing via independent manipulation of the individual nuclear spin levels. Materials with four nuclear spin levels (GaAs) and nine nuclear spin levels (InAs) offer attractive options since multibits of information can be stored and manipulated. An attractive method to manipulate the individual spin levels is introducing quadrupolar splitting, which creates a slight difference in the splitting energy of consecutive nuclear spin levels [17,41–43].

The aforesaid effects are taken into account by carefully incorporating transitions between the individually broadened nuclear spin levels using (21). A schematic of the broadened nuclear density of states and simulated conductance variation with an RF frequency sweep is shown in Figs. 8(b) and 8(c), respectively. The simulation model can be further extended to show peaks corresponding to multiphoton absorption [17,41]. Such peaks occur at higher RF powers, which induce higher rates of scattering and consequently larger broadenings of nuclear levels. This creates a density of states at energies where nuclear population is otherwise absent. Transitions corresponding to two consecutive photon absorptions can be included in our model by adding an infinitesimally small nuclear density of states in between the peaks of the nuclear density of states. Such an infinitesimally small density of states does not influence the total nuclear polarization but provides intermediate levels with extremely small lifetimes to facilitate an intermediate transition before absorbing the second photon.

A schematic diagram of nuclear density of states is shown in Fig. 8(d) where a small nuclear density of states has been added in between the main peaks to account for the multiphoton transitions. The plot of conductance versus RF frequency sweep with single-photon and multiphoton peaks is shown in Fig. 8(e). Although the magnitude of conductance change during the multiphoton processes should ideally depend on the amount of RF power being supplied, taking into account such variation requires book keeping of the details of photon density in space and the interaction between photons and nuclear spin levels. We leave these considerations for a future work.

IV. CONCLUSION

In this paper, we have developed a Landauer-Büttiker approach to understand various experimental features observed in integer quantum Hall set ups featuring QPCs. Starting from the Fermi contact hyperfine Hamiltonian, we have developed physics based models to incorporate electron-nuclear spin flip flops in to an extended Landauer-Büttiker formalism to describe the edge state electronic transport near the QPC region. This self-consistent simulation framework between the nuclear spin dynamics and edge state electronic transport aided a theoretical investigation of the hysteresis in the

conductance-voltage and RDNMR line shapes noted in certain experiments [3,11,18–20]. In particular, we demonstrated that the hysteresis noted experimentally results from a lack of quasiquilibrium between electronic transport and nuclear polarization evolution. In addition, we presented circuit models to emulate such hyperfine mediated transport effects to further facilitate a clear understanding of the electronic transport processes occurring near the QPC. Finally, we extended our models to account for the effects of quadrupolar splitting of nuclear levels and also depict the electronic transport signatures that arise from single and multiphoton processes. We believe that this work sets stage for a more rigorous approach which will include a self-consistent solution of the potential profile [44–54] of the channel along with the spatial distribution of the nuclear spin profile.

APPENDIX A: DERIVATION OF THE SPIN-FLIP TRANSMISSION COEFFICIENT

In this section, we show that the rate of spin-flip scattering from the forward propagating up-spin (down-spin) channel originating in the source contact to the forward propagating down-spin (up-spin) channel terminating in the drain contact per unit energy at the QPC can indeed be approximated by a transmission coefficient that is dependent on the nuclear polarization. The region around the QPC can be modeled by a smooth Gaussian/bell shaped potential barrier [55], which varies along the transport direction as well as along the direction perpendicular to transport. However, to model transport through a QPC, we need to know the minimum potential along the transport direction [35,55]. If both μ_D and μ_S lie above the top of the barrier, $T_{\uparrow(\downarrow)}(E) \approx 1$ in the range of energy over which electronic transport takes place. On the other hand, if the top of the barrier lie between μ_S and μ_D the channel is partially transmitted.

Let us assume that the forward propagating down-spin edge channel originating in the source contact is totally isolated from forward propagating down-spin edge channel terminating in the drain contact. A major part of the up-spin edge channel originating in the source contact is, however, transmitted through the QPC to the up-spin edge channel terminating in the drain contact. A very small portion of the electrons in the forward propagating up-spin edge channel terminating in the drain contact however suffers a spin-flip scattering at the QPC and is transmitted to the forward propagating down-spin edge channel terminating in the drain contact via electron-nuclear

spin flip-flop process. Such processes at the QPC gives rise to nuclear polarization which in turn influences electronic transport via Overhauser field.

The forward propagating up-spin edge channel near the QPC is characterized by $n_{\uparrow}^{in}(E)$ and $v_{\uparrow}(E)$, which are the density of electrons per unit energy per unit length and velocity of electrons, respectively, at the forward propagating up-spin edge channel near the QPC. Therefore

$$n_{\uparrow}^{in}(E) v_{\uparrow}(E) = \frac{1}{h}.$$

A portion of the electrons in the forward propagating up-spin edge channel is reflected, while the rest is transmitted with or without a spin-flip. Since the total current is conserved,

$$n_{\uparrow}^{in}(E) v_{\uparrow}(E) = n_{\uparrow}^{t}(E) v_{\uparrow}^{ch}(E) + n_{\uparrow}^{R}(E) v_{\uparrow}(E),$$

$$\frac{1}{h} = \frac{1}{h} T_{\uparrow}(E) + \frac{1}{h} R(E),$$

$$T_{\uparrow}(E) = 1 - R(E). \tag{A1}$$

In the above set of equations, $n_{\uparrow}^{t}(E)$ and $n_{\uparrow}^{R}(E)$ denote the density of up-spin electrons in the forward propagating edge channel at the QPC at energy E, and density of electrons that are reflected to the backward propagating edge-channel terminating in the source contact. In a similar fashion, $v_{\uparrow}^{ch}(E)$ and $v_{\uparrow}(E)$ are the group velocity of up-spin electrons in the forward propagating edge channel (terminating in the drain contact) at the QPC and the group velocity of up-spin electrons in the forward or backward propagating up-spin edge channel far away from the QPC, respectively. Assuming the QPC to be a single point, let $n_{\downarrow}^{ch}(E) v_{\downarrow}^{ch}(E)$ be the total number of electrons transmitted per unit time per unit energy at the QPC from the forward propagating up-spin edge channel terminating in the drain contact to the forward propagating down-spin edge channel terminating in the drain contact. So,

$$n_{\uparrow}^{t}(E) v_{\uparrow}^{ch}(E) = n_{\uparrow}^{ch}(E) v_{\uparrow}^{ch}(E) + n_{\downarrow}^{ch}(E) v_{\downarrow}^{ch}(E).$$

If the rate of electron-nuclear spin flip-flop at the QPC is much less compared to the rate at which electrons are transmitted from the up-spin edge channel originating in the source contact to the up-spin edge channel terminating in the drain contact through the QPC, then, $n_{\uparrow}^{ch}(E) \approx n_{\uparrow}^{t}(E)$. Our intention is to derive the approximate form for $T_{\uparrow\downarrow}^{sff}$.

The flow of electrons between the up-spin edge channel originating in the source contact to the down-spin edge channel terminating in the drain contact at the QPC is

$$
\begin{aligned}
I^{sf}(E) &= I_{\uparrow\downarrow}^{sf}(E) - I_{\downarrow\uparrow}^{sf}(E) \\
&= q N_I \times \left[\frac{3}{2} \frac{1}{2} - \frac{1}{2} - \frac{3}{2} \right] \left[\frac{dF(E)}{dt} \right]_{\text{conserving}} \\
&= q N_I \left\{ -\frac{3}{2} \Gamma_{\downarrow\uparrow}(E) F_{\frac{3}{2}} + \frac{3}{2} \Gamma_{\uparrow\downarrow}(E) F_{\frac{1}{2}} \right. \\
&\quad + \frac{1}{2} \Gamma_{\downarrow\uparrow}(E) F_{\frac{3}{2}} - \frac{1}{2} [\Gamma_{\downarrow\uparrow}(E) + \Gamma_{\uparrow\downarrow}] F_{\frac{1}{2}}(E) \\
&\quad + \frac{1}{2} \Gamma_{\uparrow\downarrow}(E) F_{-\frac{1}{2}} - \frac{1}{2} \Gamma_{\downarrow\uparrow}(E) F_{\frac{1}{2}} \\
&\quad + \left. \frac{1}{2} [\Gamma_{\downarrow\uparrow}(E) + \Gamma_{\uparrow\downarrow}(E)] F_{-\frac{1}{2}} - \frac{1}{2} \Gamma_{\uparrow\downarrow}(E) F_{-\frac{3}{2}} \right.
\end{aligned}
$$

$$-\frac{3}{2}\Gamma_{\downarrow\uparrow}(E)F_{-\frac{1}{2}} + \frac{3}{2}\Gamma_{\uparrow\downarrow}(E)F_{-\frac{3}{2}}\Bigg\}$$

$$= \{-\Gamma_{\downarrow\uparrow}(E)F_{\frac{3}{2}} + [\Gamma_{\uparrow\downarrow}(E) - \Gamma_{\downarrow\uparrow}(E)]F_{\frac{1}{2}}$$

$$+ [\Gamma_{\uparrow\downarrow}(E) - \Gamma_{\downarrow\uparrow}(E)]F_{-\frac{1}{2}} + \Gamma_{\uparrow\downarrow}(E)F_{-\frac{3}{2}}\} qN_I.$$

$$\text{(A2)}$$

$\Gamma_{\uparrow\downarrow}(E)$ and $\Gamma_{\downarrow\uparrow}(E)$ are given by

$$\Gamma_{\uparrow\downarrow}(E) = \frac{2\pi}{h} J_{\text{eff}}^2 n_\uparrow^t(E)p_\downarrow^{\text{ch}}(E),$$

$$\Gamma_{\downarrow\uparrow}(E) = \frac{2\pi}{h} J_{\text{eff}}^2 n_\downarrow^{\text{ch}}(E)p_\uparrow^t(E), \qquad \text{(A3)}$$

where

$$p_\downarrow^{\text{ch}}(E) = D_\downarrow(E) - n_\downarrow^{\text{ch}}(E),$$

$$p_\uparrow^t(E) = D_\uparrow(E) - n_\uparrow^t(E). \qquad \text{(A4)}$$

$D_\uparrow(E)$ and $D_\downarrow(E)$ are the density of states of the up-spin electrons and down-spin electrons respectively at the QPC. The Overhauser field at the QPC and the electron spin-flip tunneling is determined by the nuclear polarization which in turn is determined by the history of electron-nuclear spin

flip-flop scattering at the QPC. While electron-nuclear spin flip-flop scattering can also occur between the channels far away from the QPC terminating in the drain contact, such spin flip-flop scattering hardly causes any change in the output current as well as the Overhauser field at the QPC. We are only interested in spin-flip scattering in the vicinity of the QPC that determines the transmission coefficient of the spin-split channels. The parameter J_{eff} takes into account the spatial overlap of the density of states of the up-spin channel and the down-spin channel at the QPC. It is quite different from the parameter A_{eff} used in (5),

$$J_{\text{eff}}^2 = A_{\text{eff}}^2 \frac{\int d^3\mathbf{r}_n dE D_\uparrow(\mathbf{r}_n, E)D_\downarrow(\mathbf{r}_n, E)}{\int d^3\mathbf{r}_n dE D_\uparrow(\mathbf{r}_n, E)\int d^3\mathbf{r}_n dE D_\downarrow(\mathbf{r}_n, E)}. \quad \text{(A5)}$$

Since we are mainly interested in the spin flip-flop scattering that occur at the QPC, the range of $d^3\mathbf{r}$ includes the region at the QPC, which determines the transmission coefficients of the spin-split edge channels (narrowest region of the QPC):

$$I^{sf}(E) = I_{\uparrow\downarrow}^{sf}(E) = qn_\downarrow^{\text{ch}}(E)v_\downarrow^{\text{ch}}(E).$$

Substituting $I^{sf}(E)$ from (A2) and $p_\uparrow(E)$ and $p_\downarrow(E)$ from (A4) and doing some algebraic manipulations, we arrive at the equation

$$n_\downarrow^{\text{ch}}(E)v_\downarrow^{\text{ch}}(E) = 2\pi \frac{J_{\text{eff}}^2 N_I}{h}\{n_\uparrow^t(E)D_\downarrow(E)[F_{\frac{1}{2}} + F_{-\frac{1}{2}} + F_{-\frac{3}{2}}] - n_\downarrow^{\text{ch}}(E)D_\uparrow(E)[F_{\frac{3}{2}} + F_{\frac{1}{2}} + F_{-\frac{1}{2}}] + n_\uparrow^t(E)n_\downarrow^{\text{ch}}(E)[F_{\frac{3}{2}} - F_{-\frac{3}{2}}]\}$$

$$= 2\pi \frac{J_{\text{eff}}^2 N_I}{h}\{n_\uparrow^t(E)D_\downarrow(E)[1 - F_{\frac{3}{2}}] - n_\downarrow^{\text{ch}}(E)D_\uparrow(E)[1 - F_{-\frac{3}{2}}] + n_\uparrow^t(E)n_\downarrow^{\text{ch}}(E)[F_{\frac{3}{2}} - F_{-\frac{3}{2}}]\}$$

$$\Rightarrow n_\downarrow^{\text{ch}}(E) = \frac{2\pi \frac{J_{\text{eff}}^2 N_I}{h}n_\uparrow^t(E)D_\downarrow(E)[1 - F_{\frac{3}{2}}]}{2\pi \frac{J_{\text{eff}}^2 N_I}{h}\{n_\uparrow^t(E)[F_{-\frac{3}{2}} - F_{\frac{3}{2}}] + D_\uparrow(E)[1 - F_{-\frac{3}{2}}]\} + v_\downarrow^{\text{ch}}(E)}. \qquad \text{(A6)}$$

If the rate of spin flip-flop scattering at the QPC is slower compared to the rate of transfer of electrons between the up-spin channel originating in the source contact and the up-spin edge channel terminating in the drain contact through the QPC, that is, if $2\pi \frac{J_{\text{eff}}^2 N_I}{h}D_\uparrow(E) \ll v_\downarrow^{\text{ch}}(E)$, the first two factors in the denominator can be neglected,

$$n_\downarrow^{\text{ch}}(E) = \frac{2\pi \frac{J_{\text{eff}}^2 N_I}{h}n_\uparrow^t(E)D_\downarrow(E)(1 - F_{\frac{3}{2}})}{v_\downarrow^{\text{ch}}(E)}. \qquad \text{(A7)}$$

We assume that $n_\uparrow^t(E)$ is independent of the nuclear polarization. So,

$$n_\uparrow^{\text{ch}}(E) = \frac{T_\uparrow(E)}{hv_\uparrow^{\text{ch}}(E)}. \qquad \text{(A8)}$$

Eliminating $n_\uparrow^{\text{ch}}(E)$ from (A8) and (A7), we get

$$n_\downarrow^{\text{ch}}(E) = \frac{2\pi \frac{J_{\text{eff}}^2 N_I}{h}T_\uparrow(E)D_\downarrow(E)(1 - F_{\frac{3}{2}})}{hv_\downarrow^{\text{ch}}(E)v_\uparrow^{\text{ch}}(E)},$$

$$T_{\uparrow\downarrow}^{sff}(E) = h \times n_\downarrow^{\text{ch}}(E)v_\downarrow^{\text{ch}}(E)$$

$$= \frac{2\pi \frac{J_{\text{eff}}^2 N_I}{h}T_\uparrow(E)D_\downarrow(E)(1 - F_{\frac{3}{2}})}{v_\uparrow^{\text{ch}}(E)}$$

$$= kT_\uparrow(E)(1 - F_{\frac{3}{2}}), \qquad \text{(A9)}$$

where $k = \frac{2\pi \frac{J_{\text{eff}}^2 N_I}{h}D_\downarrow(E)}{v_\uparrow^{\text{ch}}(E)}$. Under the assumption of constant density of states over the range of energy between μ_S and μ_D, k can be taken as a constant. Similar derivations can be made to show that

$$T_{\downarrow\uparrow}^{sfb}(E) = kT_\downarrow(E)\{1 - F_{-\frac{3}{2}}\} \qquad \text{(A10)}$$

for $G > \frac{e^2}{h}$.

We call the parameter k the *spin-flip transmission coefficient*, denoted by $T_{\uparrow\downarrow}^f$ and $T_{\downarrow\uparrow}^f$ ($T_{\uparrow\downarrow}^b$ and $T_{\downarrow\uparrow}^b$) for spin-flip scattering at the QPC from forward propagating up-spin channel terminating in the drain contact to forward propagating down-spin channel terminating in the drain contact and forward propagating down-spin channel originating in the source contact to forward propagating up-spin channel terminating in the drain contact (forward propagating up-spin channel terminating in the drain contact to backward propagating down-spin channel originating in the drain contact

and forward propagating down-spin channel terminating in the drain contact to backward propagating up-spin channel originating in the drain contact) respectively. The coefficients $T_{\uparrow\downarrow}^{f}$ and $T_{\downarrow\uparrow}^{f}$ cause a change in the total charge current at the drain since the scattering occurs to a forward propagating channel. The coefficients $T_{\uparrow\downarrow}^{b}$ and $T_{\downarrow\uparrow}^{b}$, however, also cause a change in the total output current since the scattering occurs to backward propagating states. It should be noted that the above equations are only valid at the QPC in the energy range between μ_S and μ_D ($\mu_S > \mu_D$). For $E < \mu_D$, both the forward propagating and backward propagating channels are filled and hence spin-flip scattering cannot occur giving $T_{\uparrow\downarrow}^{f} = T_{\downarrow\uparrow}^{f} = T_{\uparrow\downarrow}^{b} = T_{\downarrow\uparrow}^{b} = 0$.

APPENDIX B: NONEQUILIBRIUM GREEN'S FUNCTION FORMALISM FOR CALCULATION OF CURRENT THROUGH A POTENTIAL ENERGY BARRIER

We calculate the conductance of the device by calculating the direct transmission coefficients $T_{\uparrow}$ and $T_{\downarrow}$ of the system using the nonequilibrium Green's function (NEGF) formalism assuming that the edge states of the Landau levels can be modeled as a quasi $1 - D$ ballistic conductor. Such a method of modeling has been shown to accurately match the experimental results [34,35]. We model the region of the QPC as a smooth Gaussian energy barrier [55],

$$U_O = 150 e^{-\frac{(x-x_o)^2}{2\sigma^2}} \text{ meV},$$

with $\sigma = 22$ nm and x_o is the narrowest region of the QPC that determines the transmissivity of the channels.

In case of ballistic transport in nanodevices, the generalized equations for Green's function and scattering matrices are given by the equations

$$
\begin{aligned}
G_{\uparrow(\downarrow)}(E_z) &= [E_z I - H_{\uparrow(\downarrow)} - U - \Sigma_{\uparrow(\downarrow)}(E_z)]^{-1}, \\
\Sigma_{\uparrow(\downarrow)}(E_z) &= \Sigma_{L\uparrow(\downarrow)}(E_z) + \Sigma_{R\uparrow(\downarrow)}(E_z), \\
A_{\uparrow(\downarrow)}(E_z) &= i[G_{\uparrow(\downarrow)}(E_z) - G_{\uparrow(\downarrow)}^{\dagger}(E_z)], \\
\Gamma_{L(R)\uparrow(\downarrow)}(E_z) &= [\Sigma_{L(R)\uparrow(\downarrow)}(E_z) - \Sigma_{L(R)\uparrow(\downarrow)}^{\dagger}(E_z)],
\end{aligned}
$$

(B1)

where $H_{\uparrow(\downarrow)}$ is the discretized device Hamiltonian matrix in $1 - D$ constructed using the effective mass approach [39],

$$H_{\uparrow(\downarrow)} = H_0 + U_{\uparrow(\downarrow)},$$

where H_0 is the Hamiltonian matrix in the absence of an externally applied potential at the QPC. $U_{\uparrow(\downarrow)}$ is the minimum potential energy of the electrons for the up-spin (down-spin) channel, respectively, given by (B2). U is the additional electronic potential energy due to an externally applied voltage and $\Sigma_{L\uparrow(\downarrow)}(E_z)$ and $\Sigma_{R\uparrow(\downarrow)}(E_z)$ describe the coupling and scattering of electronic wave functions due to left and right contacts respectively for the up-spin (down-spin) channel. In the above sets of equations, E_z is the free variable denoting the electronic energy along the transport direction. $A_{\uparrow(\downarrow)}(E_z)$ is the $1 - D$ spectral function and $\Gamma_{\uparrow(\downarrow)}(E_z)$ is the broadening matrix at energy E_z for the up-spin (down-spin) electrons.

The minimum potential energy of the up-spin and down-spin channels ($U_{\uparrow}$ and $U_{\downarrow}$) at the QPC are modeled by potential

barriers of the form [2]

$$U_{\uparrow} = U_O - \underbrace{\frac{g_e \mu_B B}{2}}_{\substack{\text{Zeeman} \\ \text{field}}} + \underbrace{\left(A_{\text{eff}}^{\text{Ga}} + A_{\text{eff}}^{\text{As}} \right) \frac{F_I}{2}}_{\substack{\text{Overhauser} \\ \text{field}}},$$

$$U_{\downarrow} = U_O + \overbrace{\frac{g_e \mu_B B}{2}} - \overbrace{\left(A_{\text{eff}}^{\text{Ga}} + A_{\text{eff}}^{\text{As}} \right) \frac{F_I}{2}},$$

(B2)

where $A_{\text{eff}}^{\text{Ga}}$ and $A_{\text{eff}}^{\text{As}}$ are the effective hyperfine constants for Ga and As respectively and has the respective value of $A_{\text{eff}}^{\text{Ga}} = 42 \mu\text{eV}$ and $A_{\text{eff}}^{\text{As}} = 46 \mu\text{eV}$.

The electron and hole densities per unit length at point j are given by the electron and hole correlation functions

$$n_{j\uparrow(\downarrow)} = \int \frac{[G_{\uparrow(\downarrow)}^{n}(E_z) dE_z]}{2\pi a},$$

$$p_{j\uparrow(\downarrow)} = \int \frac{[G_{\uparrow(\downarrow)}^{p}(E_z) dE_z]}{2\pi a},$$

where "a" is the lattice constant. In the above equations, $G_{\uparrow(\downarrow)}^{n}(E_z)$ and $G_{\uparrow(\downarrow)}^{p}(E_z)$ are the electron and hole correlation functions given by

$$
\begin{aligned}
G_{\uparrow(\downarrow)}^{n}(E_z) &= G_{\uparrow(\downarrow)}(E_z) \Sigma_{\uparrow(\downarrow)}^{\text{in}}(E_z) G_{\uparrow(\downarrow)}^{\dagger}(E_z), \\
G_{\uparrow(\downarrow)}^{p}(E_z) &= G_{\uparrow(\downarrow)}(E_z) \Sigma_{\uparrow(\downarrow)}^{\text{out}}(E_z) G_{\uparrow(\downarrow)}^{\dagger}(E_z),
\end{aligned}
$$

(B3)

$\Sigma^{\text{in}}(E_z)$ and $\Sigma^{\text{out}}(E_z)$ are the in-scattering and the out-scattering functions which model the rate of scattering of the electrons and holes, respectively, from the contact to the device,

$$
\begin{aligned}
\Sigma_{\uparrow(\downarrow)}^{\text{in}}(E_z) &= \Sigma_{S\uparrow(\downarrow)}^{\text{in}}(E_z) + \Sigma_{D\uparrow(\downarrow)}^{\text{in}}(E_z), \\
\Sigma_{\uparrow(\downarrow)}^{\text{out}}(E_z) &= \Sigma_{S\uparrow(\downarrow)}^{\text{out}}(E_z) + \Sigma_{D\uparrow(\downarrow)}^{\text{out}}(E_z),
\end{aligned}
$$

(B4)

where the subscript "S" and "D" denote the influence of source contact and drain contact respectively on the scattering matrices. The in-scattering and out-scattering functions are dependent on the contact quasi-Fermi distribution functions as

$$\Sigma^{in}(E_z) = \underbrace{\Gamma_S(E_z) f_S(E_z)}_{\substack{left-contact \\ inflow}} + \underbrace{\Gamma_D(E_z) f_D(E_z)}_{\substack{right-contact \\ inflow}}$$

$$\Sigma^{out}(E_z) = \underbrace{\Gamma_S(E_z)\Big\{ 1 - f_S(E_z) \Big\}}_{\substack{left-contact \\ outflow}} + \underbrace{\Gamma_D(E_z)\Big\{ 1 - f_D(E_z) \Big\}}_{\substack{right-contact \\ outflow}},$$

where $f_{S(D)}$ denote the quasi-Fermi distribution of source(drain) contact.

The direct transmission coefficients are given by

$$T_{\uparrow(\downarrow)}(E) = \text{Trace}[\Gamma_{L\uparrow(\downarrow)} G_{\uparrow(\downarrow)} \Gamma_{R\uparrow(\downarrow)} G_{\uparrow(\downarrow)}^{\dagger}]. \quad \text{(B5)}$$

The current that flows directly through the QPC from the up-spin (down-spin) edge channel originating in the source contact to the up-spin (down-spin) edge channel terminating in the drain contact (without electronic spin-flip) is given by

$$I_{\uparrow(\downarrow)} = \frac{q}{h} \int T_{\uparrow(\downarrow)}(E_z)[f_L(E_z) - f_R(E_z)] dE_z. \quad \text{(B6)}$$

APPENDIX C: DERIVATION OF [Γ]

In case, where the electronic spin-flip rate is limited by the supply of electrons from the source, $\Gamma_{\uparrow\downarrow}$ and $\Gamma_{\downarrow\uparrow}$ must be related to $|I_{\uparrow\downarrow}^{sf}|$ and $|I_{\downarrow\uparrow}^{sf}|$, respectively. We show that

$\Gamma_{\uparrow\downarrow} = C_1 |I_{\uparrow\downarrow}^{sf}|$ and $\Gamma_{\downarrow\uparrow} = C_2 |I_{\downarrow\uparrow}^{sf}|$ and solve for C_1 and C_2. We start our derivation from equation (A2). The total spin-flip current I^{sf} at the QPC can be written as the sum of up-to-down electronic spin-flip current and down-to-up electronic spin-flip current at the QPC:

$$
\begin{aligned}
I^{sf} = \int I^{sf}(E)\,dE &= qN_I \times \left[-\Gamma_{\downarrow\uparrow}F_{\frac{3}{2}} + \left\{\Gamma_{\uparrow\downarrow} - \Gamma_{\downarrow\uparrow}\right\}F_{\frac{1}{2}} + \left\{\Gamma_{\uparrow\downarrow} - \Gamma_{\downarrow\uparrow}\right\}F_{-\frac{1}{2}} + \Gamma_{\uparrow\downarrow}F_{-\frac{3}{2}} \right] \\
&= qN_I \left(\left[\Gamma_{\uparrow\downarrow}\left\{ F_{\frac{1}{2}} + F_{-\frac{1}{2}} + F_{-\frac{3}{2}} \right\} - \Gamma_{\downarrow\uparrow}\left\{ F_{\frac{3}{2}} + F_{\frac{1}{2}} + F_{-\frac{1}{2}} \right\} \right] \right) \\
&= \overbrace{qN_I \times \Gamma_{\uparrow\downarrow}\left\{ 1 - F_{\frac{3}{2}} \right\}}^{|I_{\uparrow\downarrow}^{sf}|} - \overbrace{qN_I \times \Gamma_{\downarrow\uparrow}\left\{ 1 - F_{-\frac{3}{2}} \right\}}^{|I_{\downarrow\uparrow}^{sf}|}.
\end{aligned}
$$

Let us consider the situation where $I_{\downarrow\uparrow}^{sf} = 0$. In this case, $\Gamma_{\downarrow\uparrow} = 0$,

$$
\begin{aligned}
I^{sf} &= |I_{\uparrow\downarrow}^{sf}| \\
&= qN_I \times \Gamma_{\uparrow\downarrow}\left\{ 1 - F_{\frac{3}{2}} \right\} - qN_I \times \Gamma_{\downarrow\uparrow}\left\{ 1 - F_{-\frac{3}{2}} \right\} \\
&= qN_I \Gamma_{\uparrow\downarrow}\left\{ 1 - F_{\frac{3}{2}} \right\} \\
\Gamma_{\uparrow\downarrow} &= \frac{|I_{\uparrow\downarrow}^{sf}|}{qN_I\left\{ 1 - F_{\frac{3}{2}} \right\}}.
\end{aligned}
\tag{C1}
$$

In a similar way, setting $I_{\uparrow\downarrow}^{sf} = 0$, we get

$$
\Gamma_{\downarrow\uparrow} = \frac{|I_{\downarrow\uparrow}^{sf}|}{qN_I(1 - F_{-\frac{3}{2}})}.
\tag{C2}
$$

The transition matrix [Γ] is then given by

$$
[\Gamma] = \begin{bmatrix}
-C_2|I_{\downarrow\uparrow}^{sf}| & C_1|I_{\uparrow\downarrow}^{sf}| & 0 & 0 \\
C_2|I_{\downarrow\uparrow}^{sf}| & -(C_2|I_{\downarrow\uparrow}^{sf}| + C_1|I_{\uparrow\downarrow}^{sf}|) & C_1|I_{\uparrow\downarrow}^{sf}| & 0 \\
0 & C_2|I_{\downarrow\uparrow}^{sf}| & -(C_2|I_{\downarrow\uparrow}^{sf}| + C_1|I_{\uparrow\downarrow}^{sf}|) & C_1|I_{\uparrow\downarrow}^{sf}| \\
0 & 0 & C_2|I_{\downarrow\uparrow}^{sf}| & -C_1|I_{\uparrow\downarrow}^{sf}|.
\end{bmatrix},
\tag{C3}
$$

with $C_1 = \dfrac{1}{qN_I(1 - F_{\frac{3}{2}})}$ and $C_2 = \dfrac{1}{qN_I(1 - F_{-\frac{3}{2}})}$.

APPENDIX D: DERIVATION OF [Γ_NMR] (INTERACTION BETWEEN NUCLEAR SPIN LEVELS DUE TO AN EXTERNALLY APPLIED RF FIELD)

When the nuclear spin levels are perturbed by an externally applied RF field with energy corresponding approximately to the difference in energy between the nuclear spin levels, the nuclei undergoes a periodic oscillatory transition between the consecutive spin states (Rabi oscillations [5,30]). However, due to inhomogeneities and lack of coherence in the applied RF field, the periodic oscillatory transitions decays along with an exponential decay in the nuclear polarization. Such decay time is of the order of $100\,\mu$s [4,5]. We model the temporal evolution of the nuclear polarization without taking into account such periodic oscillatory transition and calculate the occupancy of the nuclear density of states without bookkeeping of the correlation terms.

Let us assume that the applied RF frequency is ω. In steady state, the rate of transition between the sth and the $(s + 1)^{\text{th}}$

nuclear spin levels is given by [30]

$$
\begin{aligned}
&N_s(\xi)P_{s+1}(\xi + \hbar\omega)r_{s \to s+1} \\
&= N_{s+1}(\xi + \hbar\omega)P_s(\xi)r_{s+1 \to s} \\
&\Rightarrow N_I^2 D_s(\xi)F_s(\xi)D_{s+1}(\xi + \hbar\omega[1 - F_{s+1}(\xi + \hbar\omega)]r_{s \to s+1} \\
&= N_I^2 D_{s+1}(\xi + \hbar\omega)F_{s+1}(\xi + \hbar\omega)D_s(\xi)\{1 - F_s(\xi)\}r_{s+1 \to s} \\
&\Rightarrow \frac{F_s(\xi)}{1 - F_s(\xi)}\frac{1 - F_{s+1}(\xi + \hbar\omega)}{F_{s+1}(\xi + \hbar\omega)} = \frac{r_{s+1 \to s}}{r_{s \to s+1}}.
\end{aligned}
$$

In the above equations, $D_s(\xi)$, $N_s(\xi)$, $P_s(\xi)$, and $F_s(\xi)$ denote the normalized density of states of the nuclear state with spin "s" at energy ξ, density of occupied nuclear states with spin s at energy ξ, density of vacant nuclear states with spin s at energy ξ and fraction of the density of states which is occupied at energy ξ. $r_{s \to s+1}$ denote the rate at which the nuclei can undergo a transition from the nuclear state with spin $'s'$ to

the nuclear state with spin $s + 1$. In general, $r_{s \to s+1} = cN$ for stimulated absorption and $r_{s+1 \to s} = c(N + 1)$ for stimulated + spontaneous emission. N is the probability of occupancy of the bosonic density of states for photons with energy $\hbar\omega$ in equilibrium at temperature T given by $N = \frac{1}{e^{\frac{\hbar\omega}{k_B T}} - 1}$ and c is a constant of proportionality. Putting these values in the above equation, we get

$$\frac{F_s(\xi)}{1 - F_s(\xi)} \frac{1 - F_{s+1}(\xi + \hbar\omega)}{F_{s+1}(\xi + \hbar\omega)} = \frac{N + 1}{N} = e^{\frac{\hbar\omega}{k_B T}}.$$

When the nuclear spins are irradiated by an externally applied RF field of sufficient power, $N + 1 \approx N$. Hence

$$F_s(\xi) \approx F_{s+1}(\xi + \hbar\omega).$$

If the initial occupancy of the sth and $(s + 1)$th levels be denoted by F_s^0 and F_{s+1}^0, then

$$\begin{aligned} F_s(\xi) &= \frac{D_s(\xi)F_s^0(\xi) + D_{s+1}(\xi + \hbar\omega)F_{s+1}^0(\xi + \hbar\omega)}{D_s(\xi) + D_{s+1}(\xi + \hbar\omega)} \\ &= F_{s+1}(\xi + \hbar\omega). \end{aligned} \tag{D1}$$

We assume that under the influence of the perturbing RF frequency the decay of the difference in occupancy between the nuclear spin levels occurs with a time constant τ_{NMR}. Hence the rate of decay of nuclear spin polarization due to RF frequency perturbation for the case discussed above is given by

$$\begin{aligned} \frac{d}{dt}[D_s(\xi)F_s(\xi)] &= \frac{1}{\tau_{\mathrm{NMR}}} \frac{\pi\eta}{2}\big\{ D_{s+1}(\xi + \hbar\omega)D_s(\xi)F_{s+1}(\xi + \hbar\omega)[1 - F_s(\xi)] - D_{s+1}(\xi + \hbar\omega)D_s(\xi)[1 - F_{s+1}(\xi + \hbar\omega)]F_s(\xi) \big\} \\ &= \frac{1}{\tau_{\mathrm{NMR}}} \frac{\pi\eta}{2}\big\{ D_{s+1}(\xi + \hbar\omega)D_s(\xi)[F_{s+1}(\xi + \hbar\omega) - F_s(\xi)] \big\} \\ \Rightarrow \frac{d}{dt}[F_s(\xi)] &= \frac{1}{\tau_{\mathrm{NMR}}} \frac{\pi\eta}{2}\big\{ D_{s+1}(\xi + \hbar\omega)[F_{s+1}(\xi + \hbar\omega) - F_s(\xi)] \big\} \end{aligned} \tag{D2}$$

Similarly,

$$\frac{dF_{s+1}(\xi)}{dt} = \frac{1}{\tau_{\mathrm{NMR}}} \frac{\pi\eta}{2}\big\{ D_s(\xi - \hbar\omega)[F_s(\xi - \hbar\omega) - F_{s+1}(\xi)] \big\}.$$

In the above equations, the factor $\frac{\pi\eta}{2}$ acts as a normalization constant. For a nuclear system with more than two spin levels, the nuclear energy level can interact directly with the levels which energetically lie immediately above and below the level, that is, a nuclear spin level with spin s can interact directly with the levels with spins $s + 1$ and $s - 1$. The equation for time evolution occupancy of the sth nuclear spin density of states in such a case is given by:

$$\frac{dF_s(\xi)}{dt} = \frac{1}{\tau_{\mathrm{NMR}}} \frac{\pi\eta}{2}\big\{ D_{s+1}(\xi + \hbar\omega)[F_{s+1}(\xi + \hbar\omega) - F_s(\xi)] + D_{s-1}(\xi - \hbar\omega)[F_{s-1}(\xi - \hbar\omega) - F_s(\xi)] \big\}. \tag{D3}$$

For a system with four nuclear spin levels, the time evolution of the occupancy of the nuclear spin density of states under the influence of an externally applied RF field (neglecting correlation) is hence given by:

$$\left[\frac{dF(\xi)}{dt}\right]_{\mathrm{NMR}} = \mathrm{diag}\left(\frac{1}{\tau_{\mathrm{NMR}}} \frac{\pi\eta}{2}[\Gamma_{\mathrm{NMR}}(\xi)][F_{\mathrm{NMR}}(\xi, \hbar\omega)]\right),$$

where

$$\Gamma_{\mathrm{NMR}}(\xi) = \begin{bmatrix} -D_{\frac{1}{2}}(\xi - \hbar\omega) & D_{\frac{1}{2}}(\xi - \hbar\omega) & 0 & 0 \\ D_{\frac{3}{2}}(\xi + \hbar\omega) & -[D_{\frac{3}{2}}(\xi + \hbar\omega) + D_{-\frac{1}{2}}(\xi - \hbar\omega)] & D_{-\frac{1}{2}}(\xi - \hbar\omega) & 0 \\ 0 & D_{\frac{1}{2}}(\xi + \hbar\omega) & -[D_{\frac{1}{2}}(\xi + \hbar\omega) + D_{-\frac{3}{2}}(\xi - \hbar\omega)] & D_{-\frac{3}{2}}(\xi - \hbar\omega) \\ 0 & 0 & D_{-\frac{1}{2}}(\xi + \hbar\omega) & -D_{-\frac{1}{2}}(\xi + \hbar\omega) \end{bmatrix}$$

$$F_{\mathrm{NMR}}(\xi, \hbar\omega) = \begin{bmatrix} F_{\frac{3}{2}}(\xi) & F_{\frac{3}{2}}(\xi + \hbar\omega) & 0 & 0 \\ F_{\frac{1}{2}}(\xi - \hbar\omega) & F_{\frac{1}{2}}(\xi) & F_{\frac{1}{2}}(\xi + \hbar\omega) & 0 \\ 0 & F_{-\frac{1}{2}}(\xi - \hbar\omega) & F_{-\frac{1}{2}}(\xi) & F_{-\frac{1}{2}}(\xi + \hbar\omega) \\ 0 & 0 & F_{-\frac{3}{2}}(\xi - \hbar\omega) & F_{-\frac{3}{2}}(\xi) \end{bmatrix}. \tag{D4}$$

[1] Y. Hirayama, G. Yusa, K. Hashimoto, N. Kumada, T. Ota, and K. Muraki, Semicond. Sci. Technol. **24**, 023001 (2009).

[2] B. Urbaszek, X. Marie, T. Amand, O. Krebs, P. Voisin, P. Maletinsky, A. Högele, and A. Imamoglu, Rev. Mod. Phys. **85**, 79 (2013).

[3] K. R. Wald, L. P. Kouwenhoven, P. L. McEuen, N. C. van der Vaart, and C. T. Foxon, Phys. Rev. Lett. **73**, 1011 (1994).

[4] T. Machida, T. Yamazaki, and S. Komiyama, Appl. Phys. Lett. **80**, 4178 (2002).

[5] T. Machida, T. Yamazaki, K. Ikushima, and S. Komiyama, Appl. Phys. Lett. **82**, 409 (2003).

[6] A. Würtz, T. Müller, A. Lorke, D. Reuter, and A. D. Wieck, Phys. Rev. Lett. **95**, 056802 (2005).

[7] Y. Ren, W. Yu, S. M. Frolov, J. A. Folk, and W. Wegscheider, Phys. Rev. B **81**, 125330 (2010).

[8] C. R. Dean, B. A. Piot, G. Gervais, L. N. Pfeiffer, and K. W. West, Phys. Rev. B **80**, 153301 (2009).

[9] A. M. Song and P. Omling, Phys. Rev. Lett. **84**, 3145 (2000).

[10] M. Kawamura, H. Takahashi, K. Sugihara, S. Masubuchi, K. Hamaya, and T. Machida, Appl. Phys. Lett. **90**, 022102 (2007).

[11] Z. K. Keane, M. C. Godfrey, J. C. H. Chen, S. Fricke, O. Klochan, A. M. Burke, A. P. Micolich, H. E. Beere, D. A. Ritchie, K. V. Trunov, D. Reuter, A. D. Wieck, and A. R. Hamilton, Nano Lett. **11**, 3147 (2011).

[12] K. Hashimoto, K. Muraki, T. Saku, and Y. Hirayama, Phys. Rev. Lett. **88**, 176601 (2002).

[13] A. Kou, D. T. McClure, C. M. Marcus, L. N. Pfeiffer, and K. W. West, Phys. Rev. Lett. **105**, 056804 (2010).

[14] K. Akiba, S. Kanasugi, K. Nagase, and Y. Hirayama, Appl. Phys. Lett. **99**, 112106 (2011).

[15] K. Akiba, T. Yuge, S. Kanasugi, K. Nagase, and Y. Hirayama, Phys. Rev. B **87**, 235309 (2013).

[16] T. Hatano, W. Kume, S. Watanabe, K. Akiba, K. Nagase, and Y. Hirayama, Phys. Rev. B **91**, 115318 (2015).

[17] M. Kawamura, T. Yamashita, H. Takahashi, S. Masubuchi, Y. Hashimoto, S. Katsumoto, and T. Machida, Appl. Phys. Lett. **96**, 032102 (2010).

[18] G. Gervais, in *Electron Spin Resonance and Related Phenomena in Low-Dimensional Structures*, edited by M. Fanciulli (Springer, Berlin, Heidelberg, 2009), pp. 35–50.

[19] C. R. Bowers, G. M. Gusev, J. Jaroszynski, J. L. Reno, and J. A. Simmons, Phys. Rev. B **81**, 073301 (2010).

[20] L. Tiemann, T. D. Rhone, N. Shibata, and K. Muraki, Nat. Phys. **10**, 648 (2014).

[21] K. F. Yang, H. W. Liu, T. D. Mishima, M. B. Santos, K. Nagase, and Y. Hirayama, J. Phys.: Conf. Ser. **334**, 012029 (2011).

[22] K. Kodera, H. Takado, A. Endo, S. Katsumoto, and Y. Iye, Phys. Status Solidi (c) **3**, 4380 (2006).

[23] L. A. Tracy, J. P. Eisenstein, L. N. Pfeiffer, and K. W. West, Phys. Rev. B **73**, 121306 (2006).

[24] W. Desrat, D. K. Maude, M. Potemski, J. C. Portal, Z. R. Wasilewski, and G. Hill, Phys. Rev. Lett. **88**, 256807 (2002).

[25] G. Gervais, H. L. Stormer, D. C. Tsui, P. L. Kuhns, W. G. Moulton, A. P. Reyes, L. N. Pfeiffer, K. W. Baldwin, and K. W. West, Phys. Rev. Lett. **94**, 196803 (2005).

[26] M. P. Zaletel, R. S. K. Mong, F. Pollmann, and E. H. Rezayi, Phys. Rev. B **91**, 045115 (2015).

[27] J. Sakurai and J. Napolitano, *Modern Quantum Mechanics* (Pearson Education Limited, India, 2013).

[28] J. Sakurai and J. Napolitano, *Advanced Quantum Mechanics* (Pearson Education, India, 2010).

[29] D. J. Griffiths, *Introduction to Quantum Mechanics* (Pearson Education, India, 2005).

[30] C. P. Slichter, *Principles of Magnetic Resonance* (Springer-Verlag, Berlin, Heidelberg, 1990).

[31] S. Das Sarma, E. H. Hwang, and A. Kaminski, Phys. Rev. B **67**, 155201 (2003).

[32] S. Buddhiraju and B. Muralidharan, J. Phys.: Condens. Matter **26**, 485302 (2014).

[33] L. Siddiqui, A. N. M. Zainuddin, and S. Datta, J. Phys.: Condens. Matter **22**, 216002 (2010).

[34] S. Salahuddin, Ph.D. thesis, Purdue University, 2006.

[35] M. Kawamura, K. Ono, P. Stano, K. Kono, and T. Aono, Phys. Rev. Lett. **115**, 036601 (2015).

[36] J. Wan, M. Cahay, P. Debray, and R. Newrock, Phys. Rev. B **80**, 155440 (2009).

[37] R. Côté and A. M. Simoneau, Phys. Rev. B **93**, 075305 (2016).

[38] S. Datta, *Electronic Transport in Mesoscopic Systems* (Cambridge University Press, UK, 1997).

[39] S. Datta, *Quantum Transport: Atom to Transistor* (Cambridge University press, New York, 2005).

[40] S. Datta, *Lessons from Nanoelectronics: A New Perspective on Transport* (World Scientific, Singapore, 2012).

[41] G. Yusa, K. Muraki, K. Takashina, K. Hashimoto, and Y. Hirayama, Nature (London) **434**, 1001 (2005).

[42] Y. Hirayama, A. Miranowicz, T. Ota, G. Yusa, K. Muraki, S. K. Ozdemir, and N. Imoto, J. Phys.: Condens. Matter **18**, S885 (2006).

[43] A. Miranowicz, Ş. K. Özdemir, J. Bajer, G. Yusa, N. Imoto, Y. Hirayama, and F. Nori, Phys. Rev. B **92**, 075312 (2015).

[44] D. B. Chklovskii, B. I. Shklovskii, and L. I. Glazman, Phys. Rev. B **46**, 4026 (1992).

[45] A. Yacoby, T. A. Fulton, H. F. Hess, L. N. Pfei, and K. W. West, Physica E **9**, 40 (2001).

[46] J. H. Oh and R. R. Gerhardts, Phys. Rev. B **56**, 13519 (1997).

[47] K. Güven and R. R. Gerhardts, Phys. Rev. B **67**, 115327 (2003).

[48] A. Siddiki, Physica E: Low Dimens. Syst. Nanostruct. **40**, 1124 (2008).

[49] E. Papa and T. Stroh, Phys. Rev. B **75**, 045342 (2007).

[50] A. L. Efros, Phys. Rev. B **60**, 13343 (1999).

[51] R. R. Gerhardts, Phys. Status Solidi (b) **245**, 378 (2008).

[52] C. L. Kane and M. P. A. Fisher, Edge state transport, in *Perspectives in Quantum Hall Effects* (Wiley-VCH, Germany, 2007), pp. 109–159.

[53] J. R. Nikolajsen, Edge States and Contacts in the Quantum Hall Effect, Bachelor thesis, University of Copenhagen, 2013.

[54] R. R. Gerhardts, K. Panos, and J. Weis, New J. Phys. **15**, 073034 (2013).

[55] S. Arslan, E. Cicek, D. Eksi, S. Aktas, A. Weichselbaum, and A. Siddiki, Phys. Rev. B **78**, 125423 (2008).